Fizika Nizkikh Temperatur, 2006, v. 32, No. 12, p. 1522–1544

Nonequilibrium plasmons and transport properties of a double-junction quantum wire

Jaeuk U. Kim[1], Mahn-Soo Choi[2], Ilya V. Krive[3,4], and Jari M. Kinaret[3]

[1]*Department of Physics, Göteborg University, SE-412 96 Göteborg, Sweden*

[2]*Department of Physics, Korea University, Seoul 136-701, Korea*

[3]*Department of Applied Physics, Chalmers University of Technology, SE-412 96 Göteborg, Sweden*

[4]*B. Verkin Institute for Low Temperature Physics and Engineering, 47 Lenin Ave., Kharkov 61103, Ukraine*

Received January 3, 2006, revised January 22, 2006

We study theoretically the current-voltage characteristics, shot noise, and full counting statistics of a quantum wire double barrier structure. We model each wire segment by a spinless Luttinger liquid. Within the sequential tunneling approach, we describe the system's dynamics using a master equation. We show that at finite bias the nonequilibrium distribution of plasmons in the central wire segment leads to increased average current, enhanced shot noise, and full counting statistics corresponding to a super-Poissonian process. These effects are particularly pronounced in the strong interaction regime, while in the noninteracting case we recover results obtained earlier using detailed balance arguments.

PACS: 71.10.Pm, **72.70.+m**, 73.23.Hk, **73.63.–b**

Keywords: quantum wire, Luttinger liquid, shot noise, full counting statistics.

1. Introduction

The recent discovery of novel one-dimensional (1D) conductors with non-Fermi liquid behaviors has inspired extensive research activities both in theory and experiment. The generic behavior of electrons in 1D conductors is well described by the Luttinger liquid (LL) theory, a generalization of the Tomonaga–Luttinger (TL) model [1–3]. Luttinger liquids are clearly distinguished from Fermi liquids by many interesting characteristics. The most important examples among others would be (a) the bosonic nature of the elementary excitations (i.e., the collective density fluctuations) [4], (b) the power-law behavior of correlations with interaction dependent exponents [5–8], and (c) the spin-charge separation [9]. All these characteristics cast direct impacts on transport properties of an 1D system of interacting electrons, including the shot noise and the full counting statistics as we discuss in this paper.

In this paper we will consider a particular structure, namely, the single-electron transistor (SET), made of 1D quantum wires (QWs). A conventional SET with noninteracting electrodes itself is one of the most extensively studied devices in recent years in various contexts [10]. The SET of interacting 1D QWs has attracted renewed interest as a tunable device to test the LL theory and thereby improve the understanding of the 1D interacting systems. In particular, the recent experimental reports on the temperature dependence of the resonance level width in a SET of semiconductor QWs [11] and on the temperature dependence in a SWNT SET [12] stirred a controversy, with the former consistent with the conventional sequential tunneling picture [13,14] and the latter supporting the correlated sequential tunneling picture [12,15]. The issue motivated the more recent theoretical works based on a dynamical quantum Monte Carlo method [16] and on a function renormalization group method [17–20], and still remain controversial.

Another interesting issue on the SET structure of 1D QWs is the effects of the plasmon modes in the central QW [21–24]. It was suggested that the plasmon excitations in the central QW leads to a

power-law behavior of the differential conductance with sharp peaks at resonances to the plasmon modes [21]. The plasmon excitations were also ascribed to the shot noise characteristics reflecting the strong LL correlations in the device [22]. Note that in these both works, they assumed fast relaxation of plasmon excitations. We hereafter refer to this approach as «equilibrium plasmons». However, it is not clear, especially, in the presence of strong bias ($eV >> k_BT$) how well the assumption of equilibrium plasmons can be justified. This question is important since the plasmon modes excited by electron tunneling events can influence the subsequent tunnelings of electrons and hence act as an additional source of fluctuations in current. In other words, while the average conductance may not be affected significantly, the effects of the «nonequilibrium plasmons» can be substantial on shot noise characteristics [25–31]. Indeed, a recent work suggest that the nonlinear distribution of the plasmon excitations itself is of considerable interest [23] and it can affect the transport properties through the devices, especially the shot noise, significantly [23,24]. Moreover, even if the precise mechanism of plasmon relaxation in nanoscale structures is not well known and it is difficult to estimate its rate, recent computer simulations on carbon nanotubes indicate that the plasmon life time could be of the order of a picosecond, much longer than those in three-dimensional structures [32].

It is therefore valuable to investigate systematically the effects of nonequilibrium distribution of plasmon excitations with finite relaxation rate on the transport properties through a SET of 1D QWs. In this work we will focus on the shot noise (SN) characteristics and full counting statistics (FCS), which are more sensitive to the nonequilibrium plasmon excitations than average current-voltage characteristics. We found that the SN characteristics and the FCS both indicate that the fluctuations in the current through the devices is highly super-Poissonian. We ascribe this effects to the additional conduction channels via excitation of the plasmon modes. To demonstrate this rigorously, we present both analytic expression of simplified approximate models and numerical results for the full model system. Interestingly, the enhancement of the noise and hence the super-Poissonian character of the FCS is more severe in the strong interaction limit. Further more, the sensitive dependence of the super-Poissonian shot noise on the nonequilibrium plasmon excitations and their relaxation may provide a useful tool to investigate the plasmon relaxation phenomena in 1D QWs.

The paper is organized as following: In Sec. 2 we introduce our model for a 1D QW SET and briefly examine the basic properties of the tunneling rates within the golden rule approximation. We also introduce the master equation approach to be used throughout the paper, and discuss the possible experimental realizations. Before going to the main parts of the paper, in Sec. 3, we first review the results of the previous work [23], namely, the nonequilibrium distribution of the plasmons in the central QW in the limit of vanishing plasmon relaxation. This property will be useful to understand the results in the subsequent sections. We then proceed to investigate the consequence of the nonequilibrium plasmons in the context of the transport properties. We first consider average current in Sec. 4, and then discuss shot noise in Sec. 5. Finally, we investigate full counting statistics in Sec. 6. Section 7 concludes the paper.

2. Formalism

The electric transport of a double barrier structure in the (incoherent) sequential tunneling regime can be described by the master equation [14,33,34]

$$\frac{\partial}{\partial t}P(N,\{n\},t)=\sum_{N'}\sum_{\{n'\}}[\Gamma(N,\{n\}\leftarrow N',\{n'\})P(N',\{n'\},t)-\Gamma(N',\{n'\}\leftarrow N,\{n\})P(N,\{n\},t)]\,, \tag{1}$$

where $P(N,\{n\},t)$ is the probability that at time t there are N (excess) electrons and $\{n\}=(n_1, n_2, \ldots, n_m, \ldots)$ plasmon excitations (i.e., collective charge excitations), that is, n_m plasmons in the mode m on the quantum dot. The transitions occur via single-electron tunneling through the left (L) or right (R) junctions (see Fig. 1). The total transition rates Γ in master equation (1) are sums of the two transition rates Γ_L and Γ_R where $\Gamma_{L/R}(N,\{n\}\leftarrow N',\{n'\})$ is the transition rate from a quantum state $(N',\{n'\})$ to another quantum state $(N,\{n\})$ via electron tunneling through L/R-junction.

Master equation (1) implies that, with known transition rates, the occupation probabilities $P(N,\{n\},t)$ can be obtained by solving a set of linear first order differential equations with the probability conservation

$$\sum_{N,\{n\}}P(N,\{n\},t)=1.$$

In the long time limit the system converges to a steady-state with probability distribution

$$\lim_{t\to\infty} P(N,\{n\},t+\tau) = P_{\rm st}(N,\{n\}),$$

irrespective of the initial preparation of the system.

To calculate the transition rates, we start from the Hamiltonian of the system. The reservoir temperature is assumed zero ($T=0$), unless it is stated explicitly.

2.1. Model and Hamiltonian

The system we consider is a 1D quantum wire SET. Schematic description of the system is that a finite wire segment, which we call a quantum dot, is weakly coupled to two long wires as depicted in Fig. 1. The chemical potential of the quantum dot is controlled by the gate voltage (V_G) via a capacitively coupled gate electrode. In the low-energy regime, physical properties of the metallic conductors are well described by linearized dispersion relations near the Fermi points, which allows us to adopt the Tomonaga–Luttinger Hamiltonian for each wire segment. We model the system with two semi-infinite LL leads and a finite LL for the central segment. The leads are adiabatically connected to reservoirs which keep them in internal equilibria. The chemical potentials of the leads are controlled by source-drain voltage (V), and the wires are weakly coupled so that the single-electron tunneling is the dominant charge transport mechanism, i.e., we are interested in the sequential tunneling regime. Rigorously speaking, the voltage drop between the two leads (V) deviates from the voltage drop between the left and right reservoirs (say U) if electron transport is activated [35,36]. However, as long as the tunneling amplitudes through the junctions (barriers) are weak so that the Fermi golden rule approach is appropriate, we estimate $V \approx U$.

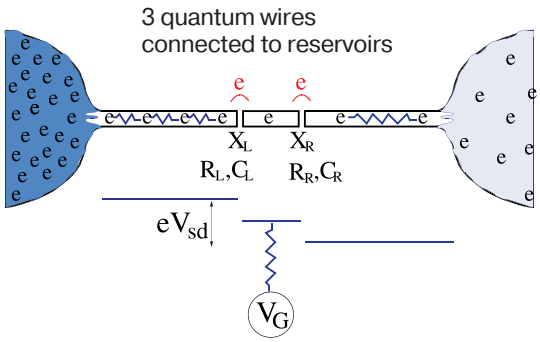

Fig. 1. Model system. Two long wires are adiabatically connected to reservoirs and a short wire is weakly coupled to the two leads. Tunneling resistances at junction points X_L and X_R are $R_{L/R}$, and the junction capacitances are considered equal $C_L = C_R$. Quantum dot is capacitively coupled to the gate electrode.

The total Hamiltonian of the system is then given by the sum of the bosonized LL Hamiltonian $\hat{H}_0 = \hat{H}_L + \hat{H}_D + \hat{H}_R$ accounting for three isolated wire segments labeled by $\ell = (L, D, R)$, and the tunneling Hamiltonian $\hat{H}_T$ accounting for single-electron hops through the junctions L and R at X_L and X_R, respectively:

$$\hat{H} = \hat{H}_0 + \hat{H}_T. \qquad (2)$$

Using standard bosonization technique, the Hamiltonian describing each wire segment can be expressed in terms of creation and annihilation operators for collective excitations ($\hat{b}^\dagger$ and $\hat{b}$) [4,37]. For the semi-infinite leads, it reads

$$\hat{H}_\ell = \sum_{\nu=1}^{M} \varepsilon_\nu^\ell \sum_{m=1}^{\infty} m \hat{b}_{\nu,m}^\dagger \hat{b}_{\nu,m} \quad \text{for} \quad \ell = L, R, \qquad (3)$$

where the index ν labels the M transport sectors of the conductor and m the wave-like collective excitations on each transport sector. The effects of the Coulomb interaction in 1D wire are characterized by the Luttinger parameter g_ν: $g=1$ for noninteracting Fermi gas and $0<g<1$ for the repulsive interactions ($g \ll 1$ in the strong interaction limit). Accordingly, the velocities of the collective excitations are also renormalized as $v_\nu = v_F/g_\nu$. The energy of an elementary excitation in sector ν is given by $\varepsilon_\nu = \pi\hbar v_\nu/L$ where L is the length of the wire and $\hbar$ the Planck constant. For instance, if the wire has a single transport channel (usually referred to as spinless electrons), e.g., a wire with one transport channel under a strong magnetic field, the system's dynamics is determined by collective charge excitations (plasmons) alone ($\nu=\rho$ and $M=1$). If, however, the spin degrees of freedom survive, the wire has two transport sectors ($M=2$); plasmons ($\nu=\rho$) and spin-waves ($\nu=\sigma$) [37]. If the system has two transport channels with electrons carrying spin ($M=4$), as is the case with SWNTs, the transport sectors are total-charge-plasmons ($\nu=\rho$), relative-charge-plasmons ($\nu=\Delta\rho$), total-spin-waves ($\nu=\rho$), and relative-spin-waves ($\nu=\Delta\sigma$) [38,39].

For the short central segment, the zero-mode need to be accounted for as well, which yields

$$\hat{H}_D = \sum_\nu \varepsilon_\nu \sum_{m=1}^{\infty} m \hat{b}_{\nu,m}^\dagger \hat{b}_{\nu,m} +$$

$$+ \frac{\varepsilon_\rho}{2Mg_\rho}(\hat{N}_\rho - N_G)^2 + \sum_{\nu\neq\rho} \frac{\varepsilon_\nu}{2Mg_\nu}\hat{N}_\nu^2 - E_r. \qquad (4)$$

In the second line of Eq. (4), which represents the zero-mode energy of the quantum dot, the operator $\hat{N}_\nu$ measures the ground-state charge, i.e., with no excitations, in the ν-sector. The zero-mode energy systematically incorporates Coulomb interaction in terms of the

Luttinger parameter g_ρ in the QD. To refer to the zero-mode energy later in this paper, we define the «charging energy» E_C as the minimum energy cost to add an excess electron to the QD in the off-Coulomb blockade regime, i.e.,

$$E_C = [E_D(2,0) - E_D(1,0)]_{N_G=1/2} = \varepsilon_\rho / g_\rho . \quad (5)$$

Note that this is twice the conventional definition, and includes the effects of finite level spacing. Hence, the charging energy is smallest in the noninteracting limit ($g_\rho = 1$) and becomes the governing energy scale in the strong interaction limit ($g_\rho << 1$). The origin of the charging energy in conventional quantum dots is the long range nature of the Coulomb interaction. In the theory of Luttinger liquid, the long range interaction can easily be incorporated microscopically through the interaction strength g_ρ. For the effect of the finite-range interaction across a tunneling junction, for instance see Refs. 40, 41.

Note that charge and spin are decoupled in Luttinger liquids, which implies the electric forces affect the (total) charge sector only; due to intrinsic $e-e$ interactions, $g_\rho < 1$ but $g_{\nu\neq\rho} = 1$, and the gate voltage shifts the band bottom of the (total) charge sector as seen by the dimensionless gate voltage parameter N_G in Eq. (4). As will be shown shortly, the transport properties of the L/R-leads are determined by the LL interaction parameter g_ρ and the number of the transport sector M. In this work, we consider each wire segment has the same interaction strength for the (total) charge sector, $g \equiv g_\rho^{(L)} = g_\rho^{(R)} = g_\rho^{(D)}$. Accordingly, the energy scales in the quantum are written by $\varepsilon_\rho \equiv \varepsilon_\rho^{(D)} = \pi\hbar v_F / g_\rho L_D$ and $\varepsilon_0 \equiv \varepsilon_{\nu\neq\rho} = \pi\hbar v_F / L_D$.

We consider the ground-state energy in the QD is the same as those in the leads, by choosing the reference energy E_r in Eq. (4) equals the minimum value of the zero-mode energy,

$$E_r = \min\left(\frac{\varepsilon_\rho N_G^2}{2Mg_\rho}, \frac{\varepsilon_\rho (1-N_G)^2}{2Mg_\rho} + \frac{\varepsilon_0 (M-1)}{2M} \right), \quad (6)$$

where $\min(x, x')$ denotes the smaller of x and x', and the gate charge N_G is in the range $N_G \in [0, M]$.

The zero-mode energy in the QD,

$$E_0 = \frac{\varepsilon_\rho}{2Mg_\rho}(N - N_G)^2 + \frac{\varepsilon_0}{2M}\sum_{\nu\neq\rho} N_\nu^2 - E_r \quad (7)$$

yields degenerate ground states for $N = 0$ and $N = 1$ excess electrons when $N_G = [(M-1)g_\rho^2 + 1]/2$. Here we replaced N_ρ by the number of the total excess electrons N since $N_\rho = N$, and N_ν are all either even or odd integers, simultaneously; in the case of the SWNTs with $N = \sum_{i,s} N_{i,s}$ excess electrons, where $i = 1, 2$ is the channel index and $s = \uparrow, \downarrow$ is the spin index of conduction electrons ($M = 4$), $N_\rho = N$,

$$N_\sigma = \sum_i (N_{i,\uparrow} - N_{i,\downarrow}),\ N_{\Delta\rho} = \sum_s (N_{1,s} - N_{2,s}),$$

$$N_{\Delta\sigma} = \sum_i (-1)^i (N_{i,\uparrow} - N_{i,\downarrow}).$$

From now on we consider only one spin-polarized (or spinless) channel unless otherwise stated — our focus is on the role of Coulomb interactions, and the additional channels only lead to more complicated excitation spectra without any qualitative change in the physics we address below. A physical realization of the single-channel case may be obtained, e.g., by exposing the quantum wire to a large magnetic field.

For the system with high tunneling barriers, the electron transport is determined by the bare electron hops at the tunneling barriers. The tunneling events in the DB structure are described by the Hamiltonian

$$\hat{H}_T = \sum_{\ell=L,R} [t_\ell \hat{\Psi}_D^\dagger(X_\ell)\hat{\Psi}_\ell(X_\ell) + \text{h.c.}] , \quad (8)$$

where $\hat{\Psi}_\ell^\dagger(X_\ell)$ and $\hat{\Psi}_\ell(X_\ell)$ are the electron creation and annihilation operators at the edges of the wires near the junctions at X_L and X_R. As mentioned earlier, the electron field operators $\hat{\Psi}$ and $\hat{\Psi}^\dagger$ are related to the plasmon creation and annihilation operators $\hat{b}$ and $\hat{b}^\dagger$ by the standard bosonization formulae. Different boundary conditions yield different relations between electron field operators and plasmon operators. Exact solutions for the periodic boundary condition have been known for decades [3,37] but the open boundary conditions which are apt for our system of consideration has been investigated only recently (see, for example, Refs. 38, 42–44).

The dc bias voltage $V = V_L + V_R$ between L and R leads is incorporated into the phase factor of the tunneling matrix elements $t_\ell = |t_\ell| \exp(\mp ieV_\ell t/\hbar)$ by a time-dependent unitary transformation [10]. Here $V_{L/R} = VC/C_{R/L}$ is voltage drop across the L/R-junction where $C = C_L C_R/(C_L + C_R)$ is the effective total capacitance of the double junction, and the bare tunneling matrix amplitudes $|t_{L/R}|$ are assumed to be energy independent. Experimentally, the tunneling matrix amplitude is sensitive to the junction properties while the capacitance is not. For simplicity, the capacitances are thus assumed to be symmetric $C_L = C_R$ throughout this work. By junction asymmetry we mean the asymmetry in (bare) squared tunneling amplitudes $|t_{L/R}|^2$. The parameter $R = |t_L|^2/|t_R|^2$ is used to describe junction asymmetry; $R = 1$ for symmetric junctions and $R >> 1$ for highly asymmetric junctions.

It is known that, at low energy scales in the quantum wires with the electron density away from

half-filling, the processes of backward and Umklapp scattering, whose processes generate momentum transfer across the Fermi sea ($\approx 2k_F$), can be safely ignored in the middle of ideal 1D conductors [37], including armchair SWNTs [38]. The Hamiltonian (2) does not include the backward and Umklapp scattering (except at the tunneling barriers) and therefore it is valid away from half-electron-filling.

We find that, in the regime where electron spin does not play a role, the addition of a transport channel does not change essential physics present in a single transport channel. Therefore, we primarily focus attention to a QW of single transport channel with spinless electrons and will comment on the effects due to multiple channel generalization, if needed.

2.2. Electron transition rates

The occupation probability of the quantum states in the SET system changes via electron tunneling events across L/R-junctions. In the single-electron tunneling regime, the bare tunneling amplitudes $|t_{L/R}|$ are small compared to the characteristic energy scales of the system and the electron tunneling is the source of small perturbation of three isolated LLs. In this regime, we calculate transition rates $\Gamma_{L/R}$ between eigenstates of the unperturbed Hamiltonian H_0 to the lowest nonvanishing order in the tunneling amplitudes $|t_{L/R}|$. In this golden rule approximation, we integrate out lead degrees of freedom since the leads are in internal equilibria, and the transition rates are given as a function of the state variables and the energies of the QD only [21,23],

$$\Gamma_{L/R}(N',\{n'\} \leftarrow N,\{n\}) = \\ = \frac{2\pi}{\hbar}|t_{L/R}|^2\,\gamma(W_{L/R})\gamma_D(\{n'\},\{n\}). \tag{9}$$

In Eq. (9) $W_{L/R}$ is the change in the Gibbs free energy associated with the tunneling across the L/R-junction,

$$W_{L/R} = E_D(N',\{n'\}) - E_D(N,\{n\}) \mp (N'-N)eV_{L/R}. \tag{10}$$

Here $E_D(N,\{n\}) = \langle N,\{n\}|\hat{H}_D|N,\{n\}\rangle$ is the energy of the eigenstate $|N,\{n\}\rangle$ of the dot and L/R correspond to $-/+$. For the QD with only one transport channel with spinless electrons only,

$$E_D(N,\{n\}) = \varepsilon_p\left[\sum_{m=1}^{\infty} m n_m + \frac{(N-N_G)^2}{2g_D}\right] - E_r\,, \tag{11}$$

where $\varepsilon_p = \varepsilon_\rho$ accounting that we consider only charge plasmons and $n_m = \langle n_m|\hat{b}_m^\dagger\hat{b}_m|n_m\rangle$ is the number of plasmons in the mode m. Note that the excitation spectrum (11) in the QD consists of *charge excitations* which are formed by changing electron number N in the zero-mode, and *plasmon excitations* which are neutral excitations. In this work, we sharply distinguish those two different excitations.

The function $\gamma(x)$ in Eq. (9) is responsible for the plasmon excitations on the leads, and given by (see, e.g., Ref. 14)

$$\gamma(\varepsilon) = \frac{1}{2\pi\hbar}\int_{-\infty}^{\infty} dt\, e^{i\varepsilon t}\langle\Psi_\ell(X_\ell,0)\Psi_\ell^\dagger(X_\ell,t)\rangle = \\ = \frac{1}{2\pi\hbar}\frac{1}{\pi v_F}\left(\frac{2\pi\Lambda g^{1/(1-g)}}{\hbar v_F\beta}\right)^{\alpha}\left|\Gamma\left(\frac{1+\alpha}{2}+i\frac{\beta\varepsilon}{2\pi}\right)\right|^2\frac{e^{-\beta\varepsilon/2}}{\Gamma(1+\alpha)}, \tag{12}$$

where $\beta = 1/k_BT$ is the inverse temperature in the leads, Λ is a short wavelength cutoff, and $\Gamma(z)$ is the gamma function. The exponent $\alpha = (g^{-1}-1)/M$ is a characteristic power law exponent indicating interaction strength of the leads with M transport sectors (hence, in our case, $M = 1$). At $g = 1$ (noninteracting case), the exponent $\alpha = 0$ and it grows as $g \to 0$ (strong interaction). The decrease of the exponent α with increasing M implies that the effective interaction decreases due to multi-channel effect, and the Luttinger liquid eventually crosses over to a Fermi liquid in the many transport channel limit [45,46].

For the noninteracting electron gas, the spectral density $\gamma(\varepsilon)$ is the TDOS multiplied by the Fermi–Dirac distribution function $f_{FD}(\varepsilon) = [1 + \exp(\beta\varepsilon)]^{-1}$; $\gamma(\varepsilon) = f_{FD}(\varepsilon)/(\pi\hbar v_F)$ for $g = 1$. At zero temperature, $\gamma(\varepsilon)$ is proportional to a power of energy,

$$\lim_{T\to 0}\gamma(\varepsilon) = \Theta(-\varepsilon)\frac{1}{\pi\hbar v_F}\frac{(|\varepsilon|/\varepsilon_\Lambda)^\alpha}{\Gamma(\alpha+1)}, \tag{13}$$

where $\varepsilon_\Lambda = \hbar v_F/\Lambda g^{1/(1-g)}$ is a high energy cut-off. At zero temperature $\gamma(\varepsilon)$ is the TDOS for the negative energies and zero otherwise (as it should be), imposed by the unit step function $\Theta(-\varepsilon)$.

The function γ_D in Eq. (9) accounts for the plasmon transition amplitudes in the QD, and is given by

$$\gamma_D(\{n'\},\{n\}) = \delta_{N',N+1}|\langle N',\{n'\}|\hat{\Psi}_D^\dagger(X_\ell)|N,\{n\}\rangle|^2 + \\ + \delta_{N',N-1}|\langle N',\{n'\}|\hat{\Psi}_D(X_\ell)|N,\{n\}\rangle|^2\,, \tag{14}$$

where we used that the zero-mode overlap is unity for $N' = N \pm 1$ and vanishes otherwise. The overlap integrals between plasmon modes are, although straightforward, quite tedious to calculate, and we refer to Appendix A for the details. The resulting overlap of the plasmon states can be written as a function of the mode occupations n_m,

$$|\langle\{n'\}|\hat{\Psi}_D^{\dagger}(X_\ell)|\{n\}\rangle|^2 = |\langle\{n'\}|\hat{\Psi}_D(X_\ell)|\{n\}\rangle|^2 =$$

$$= \frac{1}{L_D}\left(\frac{\pi\Lambda}{L_D}\right)^{\alpha_D}\phi(\{n'\},\{n\}) \qquad (15)$$

with

$$\phi(\{n'\},\{n\}) = \prod_{m=1}^{\infty}\left(\frac{1}{gm}\right)^{|n'_m-n_m|}\frac{n_m^{(<)}!}{n_m^{(>)}!}\left[L_{n_m^{(<)}}^{|n'_m-n_m|}\left(\frac{1}{gm}\right)\right]^2, \qquad (16)$$

where $n_m^{(<)} = \min(n'_m, n_m)$ and $n_m^{(>)} = \max(n'_m, n_m)$, $\alpha_D = (g_D^{-1} - 1)$ for the QD with one transport sector, and $L_a^b(x)$ are Laguerre polynomials. Additional transport sectors would appear as multiplicative factors of the same form as $\phi(\{n'\},\{n\})$ and result in a reduction of the exponent α_D. Notice that in the low energy scale only the first few occupations n_m and n'_m in the product differ from zero, participating to the transition rate (9) with nontrivial contributions.

2.3. Plasmon relaxation process in the quantum dot

In general, plasmons on the dot are excited by tunneling events and have a highly nonequilibrium distribution. The coupling of the system to the environment such as external circuit or background charge in the substrate leads to relaxation towards the equilibrium. While the precise form of the relaxation rate, Γ_p, depends on the details of the relaxation mechanism, the physical properties of our concern do not depend on the details. Here we take a phenomenological model where the plasmons are coupled to a bath of harmonic oscillators by

$$H_{\text{plasmon-bath}} = \sum_{m,n}\sum_{\alpha}(g_{mn}^{\alpha}\, b_m^{\dagger}b_n a_\alpha + \text{h.c.}). \qquad (17)$$

In Eq. (17) a_α and $a_\alpha^{\dagger}$ are bosonic operators describing the oscillator bath and g_{mn}^{α} is the coupling constants. We will assume an Ohmic form of the bath spectral density function

$$J_{mn}(\omega) \equiv \sum_{\alpha}|g_{mn}^{\alpha}|^2\,\delta(\omega-\omega_\alpha) = \gamma_p\Gamma_0\omega\,, \qquad (18)$$

where ω_α is the frequency of the oscillator corresponding to a_α, γ_p is a dimensionless constant characterizing the bath spectral density, and $\Gamma_0^{-1} = \hbar^2 v_F L_D(|t_L|^{-2} + |t_R|^{-2})$ is the natural time scale of the system. Within the rotating-wave approximation, the plasmon transition rate due to the harmonic oscillator bath is given by

$$\Gamma_p(\{n'\}\leftarrow\{n\}) = \gamma_p\Gamma_0\frac{W_p/\varepsilon_p}{e^{\beta W_p}-1} \qquad (19)$$

with

$$W_p = \varepsilon_p\sum_m(n'_m - n_m)\,,$$

where $\varepsilon_p = \varepsilon_\rho$ is the plasmon energy. Note that these phenomenological rates obey detailed balance and, therefore, at low temperatures only processes that reduce the total plasmon energy occur with appreciable rates.

2.4. Matrix formulation

For later convenience, we introduce a matrix notation for the transition rates Γ, with the matrix elements defined by

$$[\hat{\boldsymbol{\Gamma}}_\ell^{\pm}(N)]_{\{n'\},\{n\}} = \Gamma_\ell(N\pm1,\{n'\}\leftarrow N,\{n\})\,, \qquad (20)$$

i.e, the element $(\{n'\},\{n\})$ of the matrix block $\hat{\boldsymbol{\Gamma}}_\ell^{\pm}(N)$ is the transition rate $\Gamma_\ell(N\pm1,\{n'\}\leftarrow N,\{n\})$. Similarly,

$$[\hat{\boldsymbol{\Gamma}}_\ell^{0}]_{\{n'\},\{n\}} = \delta_{\{n'\},\{n\}}\sum_{\{n''\}}[\hat{\boldsymbol{\Gamma}}_\ell^{+} + \hat{\boldsymbol{\Gamma}}_\ell^{-}]_{\{n'\},\{n\}}\,, \qquad (21)$$

and

$$[\hat{\boldsymbol{\Gamma}}_p(N)]_{\{n'\},\{n\}} = -\Gamma_p(\{n'\},\{n\}) + \delta_{\{n'\},\{n\}}\sum_{\{n''\}}\Gamma_p(\{n''\},\{n\}). \qquad (22)$$

Master equation (1) can now be conveniently expressed as

$$\frac{d}{dt}|P(t)\rangle = -\hat{\boldsymbol{\Gamma}}|P(t)\rangle \qquad (23)$$

with

$$\hat{\boldsymbol{\Gamma}} = \hat{\boldsymbol{\Gamma}}_p + \sum_{\ell=L,R}(\hat{\boldsymbol{\Gamma}}_\ell^{0} - \hat{\boldsymbol{\Gamma}}_\ell^{+} - \hat{\boldsymbol{\Gamma}}_\ell^{-}),$$

where $|P(t)\rangle$ is the column vector (not to be confused with the «ket» in quantum mechanics) with elements given by $\langle N,\{n\}|P(t)\rangle \equiv P(N,\{n\},t)$. Therefore, the time evolution of the probability vector satisfies

$$|P(t)\rangle = \exp(-\hat{\boldsymbol{\Gamma}}t)|P(0)\rangle\,. \qquad (24)$$

In the long-time limit, the system reaches a steady state $|P(\infty)\rangle$.

The ensemble averages of the matrices $\hat{\boldsymbol{\Gamma}}_\ell^{\pm}$ can then be defined by

$$\langle\hat{\boldsymbol{\Gamma}}_\ell^{\pm}(t)\rangle = \sum_{N,\{n\}}\langle N,\{n\}|\hat{\boldsymbol{\Gamma}}_\ell^{\pm}|P(t)\rangle\,. \qquad (25)$$

We will construct other statistical quantities such as average current and noise power density based on Eq. (25).

3. Steady-state probability distribution of nonequilibrium plasmons

By solving the master equation (23) numerically (without plasmon relaxation), in Ref. 23, we obtained the occupation probabilities of the plasmonic many-body excitations as a function of the bias voltage and the interaction strength. We found that in the weak to noninteracting regime, $\alpha \approx 0$ or $g = 1/(1+\alpha) \approx 1$ for the wire with one transport sector, the nonequilibrium probability of plasmon excitations is a complicated function of the detailed configuration of state occupations $\{n\} = (n_1, n_2, \ldots, n_m, \ldots)$.

In contrast, the nonequilibrium occupation probability in the strong interaction regime with (nearly) symmetric tunneling barriers depends only on the total energy of the states, and follows a universal form *irrespective of electron charge N* in the QD. In the leading order approximation, it is given by

$$P^{(0)}(\varepsilon) \approx \frac{1}{Z} \exp\left(-\frac{3(\alpha+1)}{2} \frac{\varepsilon}{eV} \log \frac{\varepsilon}{\varepsilon_p} \right), \quad (26)$$

where Z is a normalization constant. Notice that ε is the total energy, including zero-mode and plasmon contributions. The distribution has a universal form which depends on the bias voltage and the interaction strength. The detailed derivation is in Appendix B. This analytic form is valid for the not too low energies $(\varepsilon, eV) \gtrsim 3\varepsilon_p$ and in the strongly interacting regime $\alpha \gtrsim 1$. More accurate approximation formula (Eq. (B.13)) is derived in Appendix B.

For symmetric junctions, the occupation probabilities fall on a single curve, well approximated by the analytic formulas Eqs. (26) and (B.13), as seen in the insets in Fig. 2, where $P(\varepsilon)$ is depicted as a function of the state energies for $g = 0.2$ (a) and $g = 0.5$ (b), with parameters $R = 1$ for the inset and $R = 100$ for the main figures ($eV = 6\varepsilon_p$, $N_G = 1/2$). For the asymmetric junctions, the line splits into several branches, one for each electric charge N, see the figure. However, as seen in Fig. 2,*a*, if the interaction is strong enough ($g \lesssim 0.3$ for $R = 100$ and $eV = 6\varepsilon_p$), each branch is, independently, well described by Eq. (26) or (B.13). For weaker interactions, $g \gtrsim 0.3$ for $R = 100$ and $eV = 6\varepsilon_p$, the analytic approximation is considerably less accurate as shown in Fig. 2,*b*. Even in the case of weaker interactions, however, the logarithms of the plasmon occupation probabilities continue to be nearly linear in ε but with a slope that deviates from that seen for symmetric junctions.

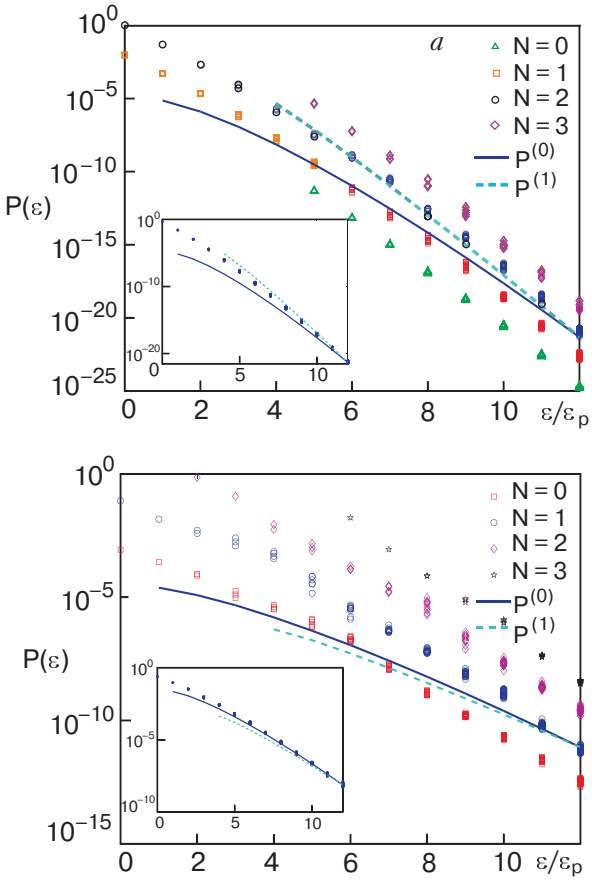

Fig. 2. The occupation occupation probability $P(\varepsilon)$ as a function of the mode energy $\varepsilon/\varepsilon_p$. The energy ε is abbreviation for $E_D(N,\{n\})$, the bias $eV = 6\varepsilon_p$, the asymmetry parameter $R = 100$, and $N_G = 1/2$ ($T = 0$). Two analytic approximations, Eq. (26) (blue curve) and Eq. (B.13) (cyan curve), are fitted to the probability distribution of the charge mode $N = 1$ (blue circle). The interaction parameter is $g = 0.2$ (a) and 0.5 (b). In the inset the case of symmetric junctions ($R = 1$) is plotted with the same conditions.

4. Average current

In terms of the tunneling current matrices across the junction L/R

$$\hat{\mathbf{I}}_{L/R} = \mp e(\hat{\boldsymbol{\Gamma}}^{+}_{L/R} - \hat{\boldsymbol{\Gamma}}^{-}_{L/R}), \quad (27)$$

the average current $I_{L/R}(t) = \langle \hat{\mathbf{I}}_{L/R}(t) \rangle$ through L/R-junction is

$$I_{L/R}(t) = \sum_{N,\{n\}} \langle N, \{n\} | \hat{\mathbf{I}}_{L/R} | P(t) \rangle . \quad (28)$$

The total external current $I(t) = \langle \hat{\mathbf{I}}(t) \rangle$, which includes the displacement currents associated with charging and discharging the capacitors at the left and right tunnel junctions, is then conveniently written as

$$I(t) = \sum_{\ell=L,R} (C/C_\ell) I_\ell(t), \qquad (29)$$

where $C^{-1} = C_L^{-1} + C_R^{-1}$. As the system reaches steady-state in the long-time limit, the charge current is conserved throughout the system, $I = I(\infty) = I_L(\infty) = I_R(\infty)$.

One consequence of nonequilibrium plasmons is the increase in current as shown in Fig. 3, where the average current is shown as a function of the bias for different interaction strengths. The currents are normalized by $I_c = I(eV = 2E_C)$ with no plasmon relaxation ($\gamma_p = 0$) for each interaction strength g, and we see that the current enhancement is substantial in the strong interaction regime ($g \lesssim 0.5$), while there is effectively no enhancement in noninteracting limit $g = 1$ (the two black lines are indistinguishable in the figure). In the weak interaction limit the current increases in discrete steps as new transport channels become energetically allowed, while at stronger interactions the steps are smeared to power laws with exponents that depend on the number of the plasmon states involved in the transport processes.

Including the spin sector results in additional peaks in the average current voltage characteristic that can be controlled by the transverse magnetic field [47,48].

The current-voltage characteristics show that, in the noninteraction limit, the nonequilibrium approach predicts similar behavior for the average current as the detailed balance approach which assumes thermal equilibrium in the QD. In contrast, in the strong interaction regime, nonequilibrium effects give rise to an enhancement of the particle current.

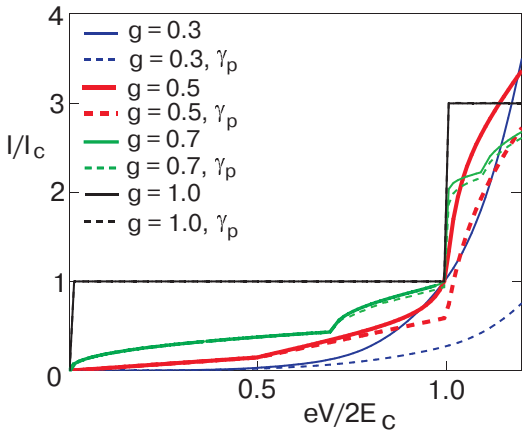

Fig. 3. Average current I/I_c as a function of the bias voltage $eV/2E_C$ and LL interaction parameter g for $R = 100$ (highly asymmetric junctions) with no plasmon relaxation ($\gamma_p = 0$, solid lines) or with fast plasmon relaxation ($\gamma_0 = 10^4$, dashed lines). The bias voltage is normalized by the charging energy $2E_C$ and current is normalized by the current at $eV = 2E_C$ with no plasmon relaxation for each g. Other parameters are $N_G = 1/2$, $T = 0$.

Experimentally, however, the current enhancement may be difficult to attribute to plasmon distribution as the current levels depend on barrier transparencies and plasmon relaxation rates, and neither of them can be easily tuned. We now turn to another experimental probe, the shot noise, which is more sensitive to nonequilibrium effects.

5. Current noise

Noise, defined by

$$S(\omega) = \lim_{t\to\infty} 2 \int_{-\infty}^{\infty} d\tau\, e^{i\omega\tau} [\langle \hat{\mathbf{I}}(t+\tau)\hat{\mathbf{I}}(t)\rangle - \langle \hat{\mathbf{I}}(t)\rangle^2], \quad (30)$$

describes the fluctuations in the current through a conductor [49,50]. Thermal fluctuations and the discreteness of the electron charge are two fundamental sources of the noise among others which are system specific [30,31]. Thermal (equilibrium) noise is not very informative since it does not provide more information than the equilibrium conductance of the system. In contrast, shot noise is a consequence of the discreteness of charge and the stochastic nature of transport. It thus can provide further insight beyond average current since it is a sensitive function of the correlation mechanism [29], internal excitations [51–53], and the statistics of the charge carriers [54–57]. Here we will particularly focus on the roles of the nonequilibrium plasmon excitations in the SETs of 1D QWs [21–24].

Within the master equation approach, the correlation functions $K_{\ell\ell'}(\tau) = \lim_{t\to\infty} \langle \hat{\mathbf{I}}_\ell(t+\tau)\hat{\mathbf{I}}_{\ell'}(t)\rangle$ in Eq. (30) can be deduced from the master equation (23). In the matrix notation they can be written as [27,28]

$$K_{\ell\ell'}(\tau) = e^2 \sum_{N,\{n\}} \langle N,\{n\}| [\Theta(+\tau)\hat{\mathbf{I}}_\ell \exp(-\hat{\Gamma}\tau)\hat{\mathbf{I}}_{\ell'} +$$

$$+ \Theta(-\tau)\hat{\mathbf{I}}_{\ell'} \exp(+\hat{\Gamma}\tau)\hat{\mathbf{I}}_\ell + \delta(\tau)\delta_{\ell\ell'}(\hat{\Gamma}_\ell^+ + \hat{\Gamma}_\ell^-)]|P(\infty)\rangle, \quad (31)$$

where $\Theta(x)$ is the unit step function. In principle, there is no well-known justification of the master equation approach, which ignores the quantum coherence effects, for the shot noise. Actually, influence of quantum coherence on shot noise is an intriguing issue [31]. However, we note that both quantum mechanical approaches [58,59] and semiclassical derivations based on a master equation approach predict identical shot noise results [26,60,61], implying that the shot noise is not sensitive to the quantum coherence in double-barrier structures. Master equation approach was used by many authors for shot noise in SET devices as well [26–28,60,62,63], and some pre-

dictions of them [27] have been experimentally confirmed [64]. On this ground, here we adopt the master equation approach and leave the precise test of the justification open to either experimental or further theoretical test.

To investigate the correlation effects, the noise power customarily compared to the Poisson value $S_{\text{Poisson}} = 2eI$. The Fano factor is defined as the ratio of the actual noise power and the Poisson value,

$$F \equiv \frac{S(0)}{2eI}. \tag{32}$$

Since thermal noise ($S = 4k_BTG(V = 0)$) is not particularly interesting, we focus on the zero frequency shot noise, in the low bias voltage regime where the Coulomb blockade governs the electric transport; $T = 0$ and $eV \lesssim 2E_C$.

5.1. Qualitative discussions

As we discuss below in detail, we have found in the absence of substantial plasmon relaxation a giant enhancement of the shot noise beyond Poissonian limit ($F = 1$) over wide ranges of bias and gate voltages; i.e., the statistics of the charge transport through the device is highly super-Poissonian. In the opposite limit of fast plasmon relaxation rate, the shot noise is reduced below the Poissonian limit (still exhibiting features specific to LL correlations) in accordance with the previous work [22]. Before going directly into details, it will be useful to provide a possible physical interpretation of the result.

We ascribe the giant super-Poissonian noise to the opening of additional conduction channels via the plasmon modes. In the parameter ranges where the giant super-Poissonian noise is observed, there are a considerable amount of plasmon excitations [23]. It means that the charges can have more than one possible paths (or, equivalently, more than two local states in the central island involved in the transport) from left to right leads, making use of different plasmon modes. Similar effects have been reported in conventional SET devices [29] and single-electron shuttles [65]. It is a rather general feature as long as the multiple transport channels are incoherent and have different tunneling rates. An interesting difference between our results and the previous results [29,65] is that the super-Poissonian noise is observed even in the sequential tunneling regime whereas in Ref. 29 it was observed in the incoherent cotunneling regime and in [65] due to the mechanical instability of the electron-mediating shuttle.

Notice that the fast plasmon relaxation prevents the additional conduction channel opening, and in the presence of fast plasmon relaxation, the device is qualitatively the same as the conventional SET. The noise is thus reduced to the Poissonian or weakly sub-Poissonian noise.

To justify our interpretation, in the following two subsections we compare two parameter regimes with only a few states involved in the transport, which are analytically tractable. When only two charge states (with no plasmon excitations) are involved (Sec. 5.2), the transport mechanism is qualitatively the same as the usual sequential tunneling in a conventional SET. Therefore, one cannot expect an enhancement of noise beyond the Poissonian limit. As the bias voltage increases, there can be one plasmon excitation associated with the lowest charging level (Sec. 5.3). In this case, through the three-state approximation, we will explicitly demonstrate that the super-Poissonian noise arises due to fluctuations induced by additional conduction channels. Detailed analysis of the full model system is provided in subsequent subsections.

5.2. Two-state model ($eV \approx \varepsilon_p$)

The electron transport involving only two lowest energy states in the quantum dot are well studied by many authors (see, for instance, Ref. 31). Nevertheless, for later reference we begin the discussion of shot noise with two-state process, which provides a reasonable approximation for $eV \approx \varepsilon_p$. At biases such that $eV \approx \varepsilon_p$ and sufficiently low temperatures, the two lowest states $|N, n_1\rangle = |0,0\rangle$ and $|1,0\rangle$ dominate the transport process and the rate matrix is given by

$$\hat{\boldsymbol{\Gamma}} = \begin{bmatrix} \gamma^+ & -\gamma^- \\ -\gamma^+ & \gamma^- \end{bmatrix}, \tag{33}$$

where the matrix elements are $\gamma^+ \equiv \Gamma_L(1,0 \leftarrow 0,0)$ and $\gamma^- \equiv \Gamma_R(0,0 \leftarrow 1,0)$.

With the current matrices defined by Eq. (27)

$$\hat{\mathbf{I}}_L = \begin{bmatrix} 0 & 0 \\ \gamma^+ & 0 \end{bmatrix}, \quad \hat{\mathbf{I}}_R = \begin{bmatrix} 0 & \gamma^- \\ 0 & 0 \end{bmatrix},$$

the noise power is obtained straightforwardly by Eqs. (30) and (31) using the steady state probability

$$|P(\infty)\rangle = \begin{bmatrix} P_{00} \\ P_{10} \end{bmatrix} = \frac{1}{\gamma^+ + \gamma^-} \begin{bmatrix} \gamma^- \\ \gamma^+ \end{bmatrix}. \tag{34}$$

The Fano factor (32) takes a simple form

$$F_2 = P_{00}^2 + P_{10}^2 = \frac{1 + (\gamma^-/\gamma^+)^2}{(1 + \gamma^-/\gamma^+)^2}, \tag{35}$$

where

$$\frac{\gamma^-}{\gamma^+} = \frac{1}{R}\left(\frac{eV/2 - \delta E_0}{eV/2 + \delta E_0}\right)^{\alpha}$$

and δE_0 is the shift of the bottom of the zero mode energy induced by the gate voltage,

$$\delta E_0 = (\delta N_G)\varepsilon_p/g, \quad \delta N_G = N_G - 1/2 \,. \quad (36)$$

Note that Eq. (36) is valid for $|\delta E_0| \le eV/2$, otherwise $I = 0$ and $S = 0$ due to Coulomb blockade. We see from Eq. (35) that the Fano factor is minimized for $\gamma^-/\gamma^+ = 1$ and maximized for $(\gamma^-/\gamma^+)^{\pm 1} = 0$, with the bounds $1/2 \le F_2 < 1$. At the gate charge $N_G = 1/2$, it is determined only by the junction asymmetry parameter R: $F_2 = (1 + R^2)/(1 + R)^2$. Note that when only two states are involved in the current carrying process (ground state to ground state transitions), the Fano factor cannot exceed the Poisson value $F = 1$.

As a consequence of the power law dependence of the transition rates on the transfer energy (13), the Fano factor is a function of the bias voltage, and the interaction strengts, it varies between the minimum and maximum values

$$F_2 = \begin{cases} \dfrac{1}{2} & \text{at } \delta E_0 = \dfrac{1 - R^{1/\alpha}}{1 + R^{1/\alpha}} \dfrac{eV}{2} \\ 1 & \text{at } \delta E_0 = \pm \dfrac{eV}{2} \end{cases} \quad (37)$$

(cf. Eq. (5) in Ref. 22). Figure 4 depicts the Fano factor as

$$N_G^{\text{dip}} = 1/2 + g(eV/2\varepsilon_p)\frac{1 - R^{1/\alpha}}{1 + R^{1/\alpha}} \,. \quad (38)$$

The Fano factor independently of the interaction strength crosses $F_2 = (1 + R^2)/(1 + R)^2$ at $N_G = 1/2$, and it approaches maximum $F_2 = 1$ at $N_G = 1/2 \pm \pm g(eV/2\varepsilon_p)$.

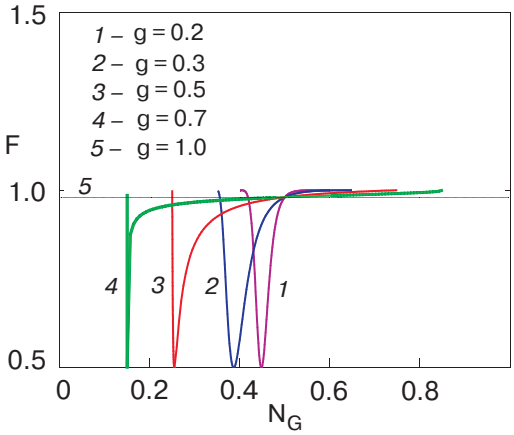

Fig. 4. Fano factor $F \equiv S(0)/2eI$ as a function of the gate charge N_G and LL interaction parameter g for R = 100 (highly asymmetric junctions) at $eV = \varepsilon_p$ ($T = 0$).

5.3. Three-state model ($eV \gtrsim 2\varepsilon_p$)

The two-state model is applicable for bias voltages below $eV_{\text{th}} = 2(\varepsilon_p - |\delta E_0|)$. Above this threshold voltage, three or more states are involved in the transport. For electron transport involving three lowest energy states in the quantum dot $|N, n_1\rangle = |0,0\rangle$, $|1,0\rangle$, and $|1,1\rangle$ with $n_m = 0$ for $m \ge 2$, the noise power can be calculated exactly if the the contribution from the (backward) transitions against the bias is negligible, as is typically the case at zero temperature. In practice, however, the backward transitions are not completely blocked for the bias above the threshold voltage of the plasmon excitations, *even at zero temperature*: once the bias voltage reaches the threshold to initiate plasmon excitations, the high-energy plasmons in the QD above the Fermi energies of the leads are also partially populated, opening the possibility of backward transitions.

A qualitatively new feature that can be studied in the three-state model as compared to the two-state model is plasmon relaxation: the system with a constant total charge may undergo transitions between different plasmon configurations.

We will show in this subsection that the analytic solution of the Fano factor of the three-state process yields an excellent agreement with the low bias numerical results in the strong interaction regime, while it shows small discrepancy in the weak interaction regime (due to non-negligible contribution from the high-energy plasmons). We will also show that within the three state model the Fano factor may exceed the Poisson value.

Analytic results

By allowing plasmon relaxation, the rate matrix involving three lowest energy states $|N, n_1\rangle = |0,0\rangle, |1,0\rangle$, and $|1,1\rangle$ is given by

$$\hat{\Gamma} = \begin{bmatrix} \gamma_0^+ + \gamma_1^+ & -\gamma_0^- & -\gamma_1^- \\ -\gamma_0^+ & \gamma_0^- & -\gamma_p \\ -\gamma_1^+ & 0 & \gamma_1^- + \gamma_p \end{bmatrix}, \quad (39)$$

with the matrix elements $\gamma_i^+ \equiv \Gamma_L(1, i \leftarrow 0,0), \gamma_i^- \equiv$ $\equiv \Gamma_R(0,0 \leftarrow 1, i)$, $i = 0,1$ and γ_p introduced in Eq. (19). Current matrices defined by Eq. (27) are

$$[\hat{\mathbf{I}}_L]_{\{2,1\}} = \gamma_0^+, \quad [\hat{\mathbf{I}}_L]_{\{3,1\}} = \gamma_1^+,$$

$$[\hat{\mathbf{I}}_R]_{\{1,2\}} = \gamma_0^-, \quad [\hat{\mathbf{I}}_R]_{\{1,3\}} = \gamma_1^-,$$

with $[\hat{\mathbf{I}}_\ell]_{\{i,j\}} = 0$ for other set of $i, j = 1, 2, 3$, where $\ell = L, R$. The noise power is obtained straightfor-

wardly by Eqs. (30) and (31) using the steady state probability

$$|P(\infty)\rangle = \begin{bmatrix} P_{00} \\ P_{10} \\ P_{11} \end{bmatrix} = \frac{1}{Z} \begin{bmatrix} \gamma_0^-(\gamma_1^- + \gamma_p) \\ \gamma_0^+(\gamma_1^- + \gamma_p) + \gamma_1^+\gamma_p \\ \gamma_1^+\gamma_0^- \end{bmatrix}, \quad (40)$$

with normalization constant $Z = \gamma_0^+\gamma_1^- + \gamma_1^+\gamma_0^- + \gamma_0^-\gamma_1^- + (\gamma_0^+ + \gamma_0^- + \gamma_1^+)\gamma_p$. Using the average current $I = e(P_{10}\gamma_0^- + P_{11}\gamma_1^-)$, the Fano factor $F = S(0)/2eI$ is given by

$$F_3 = P_{00}^2 + P_{10}^2 + P_{11}^2 + 2P_{11}\frac{1}{Z}\frac{\gamma_0^+}{\gamma_0^-} \times$$

$$\times \left[(\gamma_0^-)^2 + (\gamma_1^-)^2 - \gamma_0^-\gamma_1^- + \frac{\gamma_0^+ + \gamma_1^+}{\gamma_0^+}\gamma_1^-\gamma_p \right]. \quad (41)$$

Compared to the Fano factor (35) in the two-state process, complication arises already in the three-state process due to the last term in Eq. (41) which results from the coupling of P_{11} and the rates which cannot be expressed by the components of the probability vector.

In order to have $|N,n\rangle = |0,0\rangle$, $|1,0\rangle$, and $|1,1\rangle$ as the relevant states, we assume $\gamma_0^+ > \gamma_0^-$ or more explicitly $N_G \geq N_G^{\rm dip}$ which is introduced in Eq. (38). In the opposite situation ($\gamma_0^+ < \gamma_0^-$), the relevant states are $|N,n_1\rangle = |0,0\rangle$, $|0,1\rangle$, and $|1,0\rangle$, and the above description is still valid with the exchange of electron number $N = 0 \leftrightarrow 1$ and the corresponding notations $\gamma_i^+ \leftrightarrow \gamma_i^-$, $i = 0, 1$.

To see the implications of Eq. (41), we plot the Fano factor in Fig. 5, with respect to the gate charge N_G for symmetric junctions at $eV = 2\varepsilon_p$ ($T = 0$), with no plasmon relaxation ($\gamma_p = 0$).

Two main features are seen in Fig. 5. Firstly, the shot noise is enhanced over the Poisson limit ($F = 1$) in the strong interaction regime, $g \lesssim 0.5$, for a range of parameters with gate charges away from $N_G = 1/2$. As discussed above, in the low bias regime $eV < 2(\varepsilon_p - |\delta E_0|)$ at zero temperature, no plasmons are excited and the electric charges are transported via only the two-state process following the Fano factor (35) which results in the sub-Poissonian shot noise ($1/2 \leq F \leq 1$). Once the bias reaches the threshold $eV_{\rm th} = 2(\varepsilon_p - |\delta E_0|)$, it initiates plasmon excitations which enhance the shot noise over the Poisson limit. This feature is discussed in more detail below.

Secondly, in the weak interaction regime ($g \gtrsim 0.5$) a small discrepancy between the analytic result (41) (dashed line) and the numerical result (solid line) is found. It results from the partially populated states of the high-energy plasmons over the bias due to nonvanishing transition rates. On the other hand, a simple three-state approximation shows excellent agreement in the strong interaction regime ($g = 0.3$ in the Fig. 5), indicating negligible contribution of the high-energy plasmons ($E_D(N,\{n\}) > eV/2$) to the charge transport mechanism. This is due to the power law suppression of the transition rates (13) as a function of the transfer energy (10).

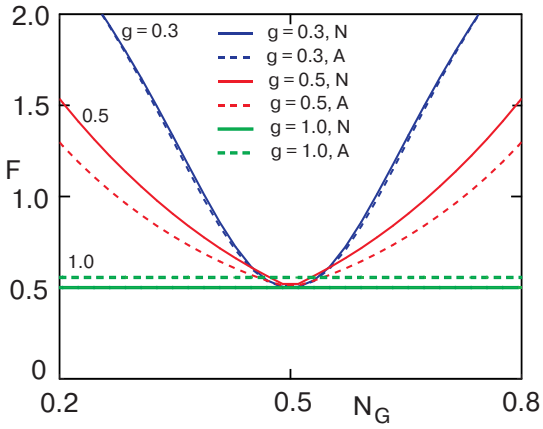

Fig. 5. Fano factor $F \equiv S(0)/2eI$ as a function of the gate charge N_G for symmetric junctions ($R = 1$) at voltage $eV = 2\varepsilon_p$ ($T = 0$) with no plasmon relaxation. Numerical results (solid lines) versus analytic results with three states, Eq. (41) (dashed lines) for $g = 0.3$, 0.5, and 1.0.

Limiting cases

To verify the role of nonequilibrium plasmons as the cause of the shot noise enhancement, we consider two limiting cases of Eq. (41): $\gamma_p = 0$ and $\gamma_p >> \gamma_i^{\pm}$.

In the limit of no plasmon relaxation ($\gamma_p = 0$), the Fano factor (41) of the three-state process is simplified as

$$F_3^{(0)} = 1 - 2[(1 - P_{10})P_{10} + (1 - P_{11})P_{11}] + 2P_{10}P_{11}\frac{(\gamma_0^-)^2 + (\gamma_1^-)^2}{\gamma_0^-\gamma_1^-}, \quad (42)$$

with steady-state probability

$$|P(\infty)\rangle = \begin{bmatrix} P_{00} \\ P_{10} \\ P_{11} \end{bmatrix} = \frac{1}{Z} \begin{bmatrix} \gamma_0^-\gamma_1^- \\ \gamma_0^+\gamma_1^- \\ \gamma_1^+\gamma_0^- \end{bmatrix}, \quad (43)$$

where the new normalization constant is $Z = \gamma_0^+\gamma_1^- + \gamma_1^+\gamma_0^- + \gamma_0^-\gamma_1^-$.

The three-state approximation is most accurate in the low bias regime $2(\varepsilon_p - |\delta E_0|) \lesssim eV << 2E_C$ (δE_0 is defined in Eq. (36)) and for gate voltages away from $N_G = 1/2$, i.e., for $1/2 < N_G \lesssim 1$ (or $0 \lesssim N_G < 1/2$ with the exchange of indices regarding particle number $N = 0 \leftrightarrow 1$) . In this regime, γ_0^+ and/or γ_1^- dominate

over the other rates, $(\gamma_0^+, \gamma_1^-) >> (\gamma_0^-, \gamma_1^+)$, which results in $1 \gtrsim P_{10} >> (P_0, P_{11}) \approx 0$. The Fano factor (42) now is reduced to

$$F_3^{(0)} \approx 1 + 2P_{10}P_{11}\frac{(\gamma_0^-)^2 + (\gamma_1^-)^2}{\gamma_0^-\gamma_1^-} \approx 1 + 2\frac{\gamma_1^+}{\gamma_0^+}. \quad (44)$$

Notice that while Eq. (42) is an exact solution for the three-state process with no plasmon relaxation, Eq. (44) is a good approximation only sufficiently far from $N_G = 1/2$. In this range, Eq. (44) explicitly shows that *the opening of new charge transport channels accompanied by the plasmon excitations causes the enhancement of the shot noise (over the Poisson limit)*.

Recently, super-Poissonian shot noises, i.e., the Fano factor $F > 1$, were found in several different situations in quantum systems. Sukhorukov et al. [29] studied the noise of the co-tunneling current through one or several quantum dots coupled by tunneling junctions, in the Coulomb blockade regime, and showed that strong inelastic co-tunneling could induce super-Poissonian shot noise due to switching between quantum states carrying currents of different strengths. Thielmann et al. [66] showed similar super-Poissonian effect in a single-level quantum dot due to spin-flip co-tunneling processes, with a sensitive dependence on the coupling strength. The electron spin in a quantum dot in the Coulomb blockade regime can generate super-Poissonian shot noise also at high frequencies [67]. The shot noise enhancement over the Poisson limit can be observed by studying the resonant tunneling through localized states in a tunnel-barrier, resulting from Coulomb interaction between the localized states [68]. In nano-electro-mechanical systems, in the semiclassical limit, the Fano factor exceeds the Poisson limit at the shuttle threshold [65,69]. Commonly, the super-Poissonian shot noise is accompanied by internal instability or a multi-channel process in the course of electrical transport.

In the limit of fast plasmon relaxation, on the other hand, $\gamma_p >> \gamma_i^{\pm}$ and effectively no plasmon is excited,

$$|P(\infty)\rangle \approx \begin{bmatrix} P_{00} \\ P_{10} \\ P_{11} \end{bmatrix} = \frac{1}{\gamma_0^+ + \gamma_1^+ + \gamma_0^-} \begin{bmatrix} \gamma_0^- \\ \gamma_0^+ + \gamma_1^+ \\ 0 \end{bmatrix}. \quad (45)$$

Consequently, the Fano factor (41) is given by

$$F_3^{(\infty)} \approx \frac{1}{2} + 2\left(P_{00} - \frac{1}{2}\right)^2 \in \left[\frac{1}{2}, 1\right]. \quad (46)$$

The maximum Fano factor $F = 1$ is reached if one of the rates γ_0^+ or γ_0^- dominates, while the minimum value $F = 1/2$ requires that $\gamma_0^- = \gamma_0^+ + \gamma_1^+$, i.e., that the total tunneling-in and tunneling-out rates are equal; more explicitly,

$$\frac{1}{R}\left(1 - \frac{2\delta E_0}{eV/2 + \delta E_0}\right)^{\alpha} - \frac{1}{g}\left(1 - \frac{\varepsilon_p}{eV/2 + \delta E_0}\right)^{\alpha} = 1. \quad (47)$$

5.4. Numerical results

The limiting cases of no plasmon relaxation ($\gamma_p = 0$) and a fast plasmon relaxation ($\gamma_p = 10^4$) are summarized in Fig. 6,*a* and *b*, respectively. In the figure the Fano factor is plotted as a function of gate voltage and interaction parameter g in the strong interaction regime $0.3 \le g \le 0.6$ at $eV = 2\varepsilon_p$ for $R = 100$ (strongly asymmetric junctions).

As shown in Fig. 6,*a*, the Fano factor is enhanced above the Poisson limit ($F = 1$) for a range of gate charges not very close to $N_G = 1/2$, especially in the strong interaction regime, as expected from the three-state model. The shot noise enhancement is lost in the presence of a fast plasmon relaxation process, in agreement with analytic arguments, as seen in Fig. 6,*b* when F is bounded by $1/2 \le F \le 1$. Hence, *slowly re-*

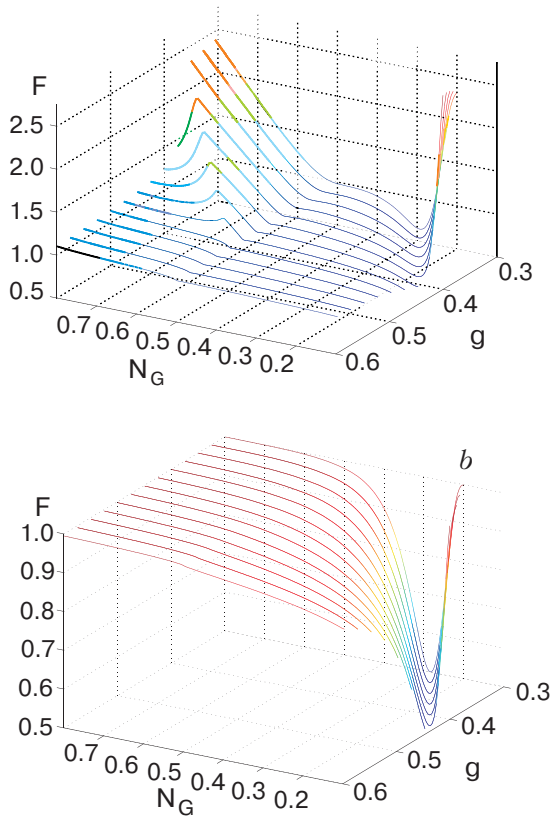

Fig. 6. Fano factor $F \equiv S(0)/2eI$ as a function of the gate charge N_G and LL interaction parameter g for $R = 100$ (highly asymmetric junctions) at $eV = 2\varepsilon_p$ ($T = 0$), with no plasmon relaxation ($\gamma_p = 0$) (*a*) and with fast plasmon relaxation ($\gamma_p = 10^4$) (*b*).

laxing plasmon excitations enhance shot noise, and this enhancement is most pronounced in the strongly interacting regime.

In the limit of fast plasmon relaxation F exhibits a minimum value $F = 1/2$ at positions consistent with predictions of the three-state model: the voltage polarity and ratio of tunneling matrix elements at the two junctions is such that total tunneling-in and tunneling-out rates are roughly equal for small values of N_G. If plasmon relaxation is slow, F still has minima at approximately same values of N_G but the minimal value of the Fano factor is considerably larger due to the presence of several transport channels.

5.5. Interplay between several charge states and plasmon excitations near $eV = 2E_C$

So far, we have investigated the role of nonequilibrium plasmons as the cause of the shot noise enhancement and focused on a voltage range when only two charge states are significantly involved in transport. The question naturally follows what is the consequence of the involvement of several charge states. Do they enhance shot noise, too?

To answer this question, we first consider a toy model in which the plasmon excitations are absent during the single-charge transport. In the three-N-state regime where the relevant states are $|N\rangle = |-1\rangle$, $|0\rangle$ and $|1\rangle$ with no plasmon excitations at all. At zero temperature, the rate matrix in this regime is given by

$$\hat{\Gamma} = \begin{bmatrix} \Gamma_{-1}^{+} & -\Gamma_{0}^{-} & 0 \\ -\Gamma_{-1}^{+} & \Gamma_{0}^{-} + \Gamma_{0}^{+} & -\Gamma_{1}^{-} \\ 0 & -\Gamma_{0}^{+} & \Gamma_{1}^{-} \end{bmatrix}, \qquad (48)$$

where the matrix elements are

$$\Gamma_i^+ = \Gamma_L(i+1, \{0\} \leftarrow i, \{0\}),$$

$$\Gamma_i^- = \Gamma_R(i-1, \{0\} \leftarrow i, 0), \quad i = -1, 0, 1.$$

Repeating the procedure in Sec. 5.3, we arrive at a Fano factor that has a similar form as Eq. (42),

$$F_{3N} = 1 - 2[(1-P_{-1})P_{-1} + (1-P_1)P_1] + \\ + 2P_{-1}P_1\left(\frac{\Gamma_{-1}^{+}}{\Gamma_1^{-}} + \frac{\Gamma_1^{-}}{\Gamma_{-1}^{+}}\right), \qquad (49)$$

with the steady-state probability vector

$$|P(\infty)\rangle = \begin{bmatrix} P_{-1} \\ P_0 \\ P \end{bmatrix} = \frac{1}{Z}\begin{bmatrix} \Gamma_0^-\Gamma_1^- \\ \Gamma_{-1}^+\Gamma_1^- \\ \Gamma_{-1}^+\Gamma_0^+ \end{bmatrix}, \qquad (50)$$

where $Z = \Gamma_0^-\Gamma_1^- + \Gamma_{-1}^+\Gamma_1^- + \Gamma_{-1}^+\Gamma_0^+$.

Despite the formal similarity of Eq. (49) with Eq. (42), its implication is quite different. In terms of the transition rates, F_{3N} reads

$$F_{3N} = 1 - \frac{2}{Z^2}\left[\Gamma_1^-\Gamma_0^-(\Gamma_{-1}^+\Gamma_0^+ + (\Gamma_{-1}^+ - \Gamma_0^+)\Gamma_1^-) + \right. \\ \left. + \Gamma_{-1}^+\Gamma_0^+(\Gamma_0^-\Gamma_1^- + (\Gamma_1^- - \Gamma_0^-)\Gamma_1^-)\right]. \qquad (51)$$

Since $\Gamma_{-1}^+ > \Gamma_0^+$ and $\Gamma_1^- > \Gamma_0^-$ in the three-N-state regime, the Fano factor F_{3N} is sub-Poissonian, i.e., $F_{3N} < 1$, consistent with the conventional equilibrium descriptions [22,27].

We conclude that while plasmon excitations may enhance the shot noise over the Poisson limit, the involvement of several charge states and the ensuing correlations, in contrast, do not alter the sub-Poissonian nature of the Fano factor in the low-energy regime. This qualitative difference is due to the fact that certain transition rates between different charge states vanish identically (in the absence of co-tunneling): it is impossible for the system to move directly from a state with $N = -1$ to $N = 1$ or vice versa.

Therefore, we expect that for bias voltages near $eV = 2E_C > 2\varepsilon_p$, when both plasmon excitations and several charge excitations are relevant, the Fano factor will exhibit complicated nonmonotonic behavior. Exact solution is not tractable in this regime since it involves too many states. Instead, we calculate the shot noise numerically, with results depicted in Fig. 7, where the zero temperature Fano factor is shown as a function of the bias eV and LL interaction parameter g for $R = 100$ at $N_G = 1/2$, (*a*) with no plasmon relaxation ($\gamma_p = 0$) and (*b*) with fast plasmon relaxation ($\gamma_p = 10^4$).

In the bias regime up to the charging energy $eV \le 2E_C$, the Fano factor increases monotonically due to nonequilibrium plasmons. On the other hand, additional charge states contribute at $eV \ge 2E_C$ which tends to suppress the Fano factor. As a consequence of this competition, the Fano factor reaches its peak at $eV = 2E_C$ and is followed by a steep decrease as shown in Fig. 7,*a*. Note the significant enhancement of the Fano factor in the strong interaction regime, which is due in part to the power law dependence of the transition rates with exponent $\alpha = (1/g - 1)$ as discussed earlier, and in part to more plasmon states being involved for smaller g since $E_C = \varepsilon_p/g$. The latter reason also accounts for the fact that the Fano factor begins to rise at a lower apparent bias for smaller g: the bias voltage is normalized by E_C so that plasmon excitation is possible for lower values of eV/E_C for stronger interactions.

In the case of fast plasmon relaxation, the rich structure of the Fano factor due to nonequilibrium

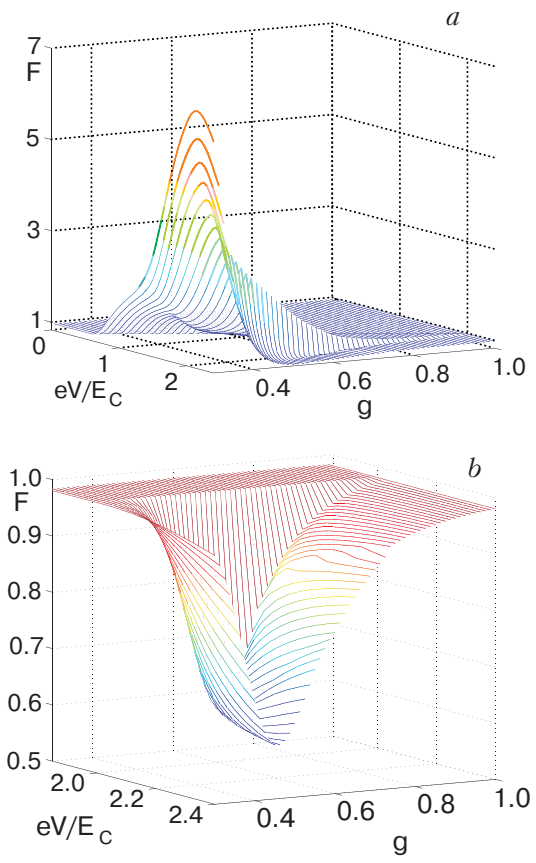

Fig. 7. Fano factor $F \equiv S(0)/2eI$ as a function of the bias eV and LL interaction parameter g for $R = 100$ (highly asymmetric junctions) at $N_G = 1/2$ ($T = 0$): with no plasmon relaxation ($\gamma_p = 0$) (*a*) and with fast plasmon relaxation ($\gamma_p = 10^4$) (*b*).

plasmons is absent as shown in Fig. 7,*b*, in agreement with the discussions in previous subsections. The only remaining structure is a sharp dip around $eV = 2E_C$ that can be attributed to the involvement of additional charge states at $eV \geq 2E_C$. Not only the minimum value of the Fano factor is a function of the interaction strength but also the bias voltage at which it occurs depends on g. The minimum Fano factor occurs at higher bias voltage, and the dip tends to be deeper with increasing interaction strength. Note for $g \lesssim 0.5$, the Fano factor did not reach its minimum still at largest voltages plotted ($eV/2E_C = 1.2$).

The Fano factor at very low voltages $eV < 2\varepsilon_p$ for $N_G = 1/2$ is $F^{(0)} = (1 + R^2)/(1 + R)^2$ (see Eq. (35)), regardless of the plasmon relaxation mechanism. As shown in Fig. 7,*b*, the Fano factor is bounded above by this value in the case of fast plasmon relaxation. Notice that in the case of no plasmon relaxation (Fig. 7,*a*), the dips in the Fano factor at $eV > 2E_C$ reach below $F^{(0)}$. See Fig. 1,*a* in Ref. 24 for more detail.

Since both the minimum value of F and the voltage at which it occurs are determined by a competition between charge excitations and plasmonic excitations, they cannot be accurately predicted by any of the simple analytic models discussed above.

6. Full counting statistics

Since shot noise, that is a current-current correlation, is more informative than the average current, we expect even more information with higher-order currents or charge correlations. The method of counting statistics, which was introduced to mesoscopic physics by Levitov and Lesovik [70] followed by Muzykantskii and Khmelnitskii [71] and Lee et al. [72], shows that all orders of charge correlation functions can be obtained as a function related to the probability distribution of transported electrons for a given time interval. This powerful approach is known as full counting statistics (FCS). The first experimental study of the third cumulant of the voltage fluctuations in a tunnel junction was carried out by Reulet et al. [73]. The experiment indicates that the higher cumulants are more sensitive to the coupling of the system to the electromagnetic environment. See also Refs. 74, 75 for the theoretical discussions on the third cumulant in a tunnel-barrier.

We will now carry out a FCS analysis of transport through a double barrier quantum wire system. The analysis will provide a more complete characterization of the transport properties of the system than either average current or shot noise, and shed further light on the role of nonequilibrium versus equilibrium plasmon distribution in this structure.

Let $P(M, \tau)$ be the probability that M electrons have tunneled across the right junction to the right lead during the time τ. We note that

$$P(M,\tau) =$$

$$= \lim_{t\to\infty} \sum_{N,\{n\}} \sum_{M_0,N_0,\{n_0\}} P(M_0 + M, N, \{n\}, t + \tau; M_0, N_0, \{n_0\}, t),$$

where $P(M_0 + M, N, \{n\}, t + \tau; M_0, N_0, \{n_0\}, t)$ is called joint probability since it is the probability *that*, up to time t, M_0 electrons have passed across the right junction and N_0 electrons are confined in the QD with $\{n_0\}$ plasmon excitations, *and that* $M_0 + M$ electrons have passed R-junction with $(N, \{n\})$ excitations in the QD up to time $t + \tau$. The master equation for the joint probability can easily be constructed from Eq. (23) by noting that $M \to M \pm 1$ as $N \to N \mp 1$ via only R-junction hopping

To obtain $P(M, \tau)$, it is convenient to define the characteristic function conjugate to the joint probability as

$$g(\theta, N, \{n\}, \tau) =$$

$$= \lim_{t\to\infty} \sum_M e^{-i\theta M} \sum_{M_0,N_0,\{n_0\}} P(M_0+M,N,\{n\},t+\tau;M_0,N_0,\{n_0\},t).$$

The characteristic function satisfies the master equation

$$\frac{\partial}{\partial\tau}|g(\theta,\tau)\rangle = -\hat{\boldsymbol{\Gamma}}(\theta)|g(\theta,\tau)\rangle$$

with the initial condition $|g(\theta,\tau=0)\rangle = |P(\infty)\rangle$. The θ-dependent $\hat{\boldsymbol{\Gamma}}$ in Eq. (52) is related to the previously defined transition rate matrices through

$$\hat{\boldsymbol{\Gamma}}(\theta) = \hat{\Gamma}_p + (\hat{\boldsymbol{\Gamma}}_L^0 - \hat{\boldsymbol{\Gamma}}_L^+ - \hat{\boldsymbol{\Gamma}}_L^-) + \\ + (\hat{\boldsymbol{\Gamma}}_R^0 - \hat{\boldsymbol{\Gamma}}_R^+ e^{i\theta} - \hat{\boldsymbol{\Gamma}}_R^- e^{-i\theta}). \quad (53)$$

The characteristic function $G(\theta,\tau)$ conjugate to $P(M,\tau)$ is now given by $G(\theta,\tau) = \sum_{N,\{n\}} \langle N,\{n\}|g(\theta,\tau)\rangle$, or

$$G(\theta,\tau) = \sum_{N,\{n\}} \langle N,\{n\}|\exp[-\hat{\boldsymbol{\Gamma}}(\theta)\tau]|P(\infty)\rangle . \quad (54)$$

Finally, the probability $P(M,\tau)$ is obtained by

$$P(M,\tau) = \int_0^{2\pi} \frac{d\theta}{2\pi} e^{i\theta M} G(\theta,\tau) = \oint \frac{dz}{2\pi i} \frac{G(z,\tau)}{z^{2M+1}} \quad (55)$$

with $z = e^{-i\theta/2}$, where the contour runs counterclockwise along the unit circle and we have used the symmetry property $G(z,\tau) = G(-z,\tau)$ for the second equality.

Taylor expansion of the logarithm of the characteristic function in $i\theta$ defines the *cumulants* or irreducible correlators $\kappa_k(\tau)$:

$$\ln G(\theta,\tau) = \sum_{k=1}^{\infty} \frac{(i\theta)^k}{k!} \kappa_k(\tau) . \quad (56)$$

The cumulants have a direct polynomial relation with the moments $\overline{n^k(\tau)} \equiv \sum_n n^k P(n,\tau)$. The first two cumulants are the mean and the variance, and the third cumulant characterizes the asymmetry (or skewness) of the $P(M,\tau)$ distribution and is given by

$$\kappa_3(\tau) = \overline{\delta n(\tau)^3} = \overline{(n(\tau) - \overline{n(\tau)})^3} . \quad (57)$$

In this section, we investigate FCS mainly in the context of the probability $P(M,\tau)$ that M electrons have passed through the right junction during the time τ. Since the average current and the shot noise are proportional to the average number of the tunneling electrons $\langle M\rangle$ and the width of the distribution of $P(M,\tau)$, respectively, we focus on the new aspects that are not covered by the study of the average current or shot noise.

In order to get FCS in general cases we integrate the master equation (52) numerically (see Sec. 6.3). In the low-bias regime, however, some analytic calculations can be made. We will show through the following subsections that for symmetric junctions in the low-bias regime ($2\varepsilon_p < eV < 2E_C$), and irrespective of the junction symmetry in the very low bias regime ($eV < 2\varepsilon_p$), $P(M,\tau)$ is given by the residue at $z=0$ alone,

$$P(M,\tau) = \frac{1}{(2M)!} \left.\frac{d^{2M}}{dz^{2M}}\right|_{z=0} G(z,\tau) . \quad (58)$$

Through this section we assume that the gate charge is $N_G = 1/2$, unless stated explicitly not so.

We will now follow the outline of the previous section and start by considering two analytically tractable cases before proceeding with the full numerical results.

6.1. Two-state process; $eV \approx \varepsilon_p$

For the very low bias $eV < 2\varepsilon_p$ at zero temperature, no plasmons are excited and electrons are carried by transitions between two states $(N,n) = (0,0) \leftrightarrow (1,0)$. In this simplest case, the rate matrix $\hat{\boldsymbol{\Gamma}}(\theta)$ in Eq. (52) is determined by only two participating transition rates $\gamma^+ = \Gamma_L(1,0 \leftarrow 0,0)$ and $\gamma^- = \Gamma_R(0,0 \leftarrow 1,0)$,

$$\hat{\boldsymbol{\Gamma}}(\theta) = \begin{bmatrix} \Gamma_0 + \delta & -(\Gamma_0 - \delta) e^{-i\theta} \\ -(\Gamma_0 + \delta) & \Gamma_0 - \delta \end{bmatrix} \quad (59)$$

with $\Gamma_0 \equiv (\gamma^+ + \gamma^-)/2$, $\delta \equiv (\gamma^+ - \gamma^-)/2$.

Substituting the steady-state probability Eq. (34) and the transition rate matrix (59) to Eq. (54), one finds

$$G_2(z,\tau) = \frac{e^{-\Gamma_0\tau}}{4} \frac{1}{f_2(z)} [(1+f_2(z))^2 e^{\Gamma_0\tau f_2(z)} - \\ - (1-f_2(z))^2 e^{-\Gamma_0\tau f_2(z)}], \quad (60)$$

where $f_2(z) = (\Gamma_\delta/\Gamma_0)\sqrt{z^2+\Delta^2}$, with $\Gamma_\delta = \sqrt{\Gamma_0^2 - \delta^2} = \sqrt{\gamma^+\gamma^-}$ and $\Delta^2 = \delta^2/\Gamma_\delta^2$.

Now, it is straightforward to calculate the cumulants. In the long time limit $\tau >> (\gamma^\pm)^{-1}$, for instance, in terms of the average current $I_2 = e\gamma^+\gamma^-/(\gamma^+ + \gamma^-)$ and the Fano factor F_2 in (35), the three lowest cumulants are given by

$$\kappa_1(\tau) = I_2\tau, \quad \kappa_2(\tau) = eI_2F_2\tau, \\ \kappa_3(\tau) = e^2I_2[3(F_2 - 1/2)^2 + 1/4]\tau , \quad (61)$$

where the electron charge $(-e)$ is revived. These are in agreement with the phase-coherent quantum-mechanical results [76]. It is convenient to discuss the asym-

metry (skewness) by the ratio $A \equiv \kappa_3/e^2\kappa_1$ ($\tau \to \infty$), noticing the Fano factor $F = \lim \kappa_2(\tau)/e\kappa_1(\tau)$. The factor $A_2 = 3(F_2 - 1/2)^2 + 1/4$ is positive definite (positive skewness) and bounded by $1/4 \le A_2 \le 1$. It is interesting to notice that A_2 is a monotonic function of F_2 and has its minimum $A_2 = 1/4$ for the minimum $F_2 = 1/2$ and maximum $A_2 = 1$ for the maximum $F_2 = 1$. Notice $A = 1$ for a Poissonian and $A = 0$ for a Gaussian distribution. Therefore, the dependence of A_2 on the gate charge N_G is similar to that of the Fano factor F_2 (see Fig. 4) with dips at $N_G^{\rm dip}$ in Eq. (38). Together with Eq. (37), it implies that the effective shot noise and the asymmetry of the probability distribution per unit charge transfer have their respective minimum values at the gate charge $N_G^{\rm dip}$ which depends on the tunnel-junction asymmetry and the interaction strength of the leads.

The integral in Eq. (55) is along the contour depicted in Fig. 8. Notice that the contributions from the part along the branch cuts are zero and we are left with the multiple poles at $z = 0$. By residue theorem, the two-state probability $P_2(M,\tau)$ is given by Eq. (58).

The exact expression of $P_2(M,\tau)$ is cumbersome. For symmetric tunneling barriers with $N_G = 1/2$ ($\delta = 0$, $\gamma^+ = \gamma^- = \Gamma_0$), however, Eq. (60) is reduced to

$$G_2^{(s)}(z,\tau) = \frac{e^{-\Gamma_0\tau}}{4z}\left[(1+z)^2 e^{\Gamma_0\tau z} - (1-z)^2 e^{-\Gamma_0\tau z}\right]. \tag{62}$$

Accordingly, $P_2^{(s)}(M,\tau)$ is concisely given by

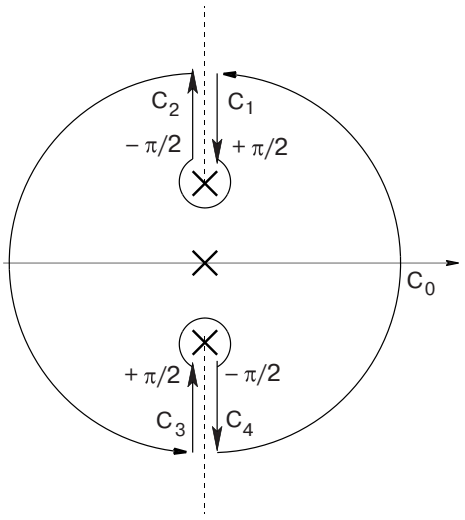

Fig. 8. Contour of Eq. (55). The arguments of $f_2(z) = (\Gamma_\delta/\Gamma_0)\sqrt{z^2+\Delta^2}$ are $\pi/2$, $-\pi/2$, $\pi/2$, $-\pi/2$ along the branch cuts C_1, C_2, C_3, and C_4, respectively.

$$P_2^{(s)}(M,\tau) = e^{-\Gamma_0\tau}\left[\frac{1}{2}\frac{(\Gamma_0\tau)^{2M-1}}{(2M-1)!} + \frac{(\Gamma_0\tau)^{2M}}{(2M)!} + \frac{1}{2}\frac{(\Gamma_0\tau)^{2M+1}}{(2M+1)!}\right] \quad \text{for } M \ge 1, \tag{63}$$

with $P_2^{(s)}(0,\tau) = e^{-\Gamma_0\tau}(1 + \Gamma_0\tau/2)$, in agreement with Eq. (24) of Ref. 76. While this distribution resembles a sum of three Poisson distributions, it is not exactly Poissonian.

For a highly asymmetric junctions $R >> 1$ ($\gamma^+ >> \gamma^-$), the first term in Eq. (60) dominates the dynamics of $G_2(z,\tau)$ and its derivatives, and the characteristic function is approximated by

$$G_2^{(a)}(z,\tau) \approx \exp\left(-\tau\Gamma_0 + \tau\sqrt{(\gamma^+\gamma^-)z^2 + \delta^2}\right). \tag{64}$$

Now, the solution of $P_2^{(a)}(M,\tau)$ is calculated by this equation and Eq. (58). The leading order approximation in γ^-/γ^+ leads to the Poisson distribution,

$$P_2^{(a)}(M,\tau) \approx \frac{(\gamma^-\tau)^M}{M!} e^{-\gamma^-\tau}. \tag{65}$$

For a single tunneling-barrier, the charges are transported by the Poisson process ($F = 1$) [31]. Therefore, we recover the Poisson distribution in the limit of strongly asymmetric junctions and in the regime of the two-state process, in which electrons see effectively single tunnel-barrier.

For the intermediate barrier asymmetry the probability $P_2(M,\tau)$ of a two-state process is given by a distribution between Eq. (63) (for symmetric junctions) and the Poissonian (65) (for the most asymmetric junctions).

6.2. Four-state process; $2\varepsilon_p \lesssim eV \lesssim 2E_C$

Since we focus the FCS analysis on the case $N_G = 1/2$, the next simplest case to study is a four-state-model rather than the three-state-model discussed in the connection of the shot noise in the previous section.

In the bias regime where the transport is governed by Coulomb blockade ($eV < 2E_C$) and yet the plasmons play an important role ($eV \ge 2\varepsilon_p$), it is a fairly good approximation to include only the four states with $N = 0,1$ and $n_1 = 0,1$ ($n_m = 0$ for $m \ge 2$). For general asymmetric cases, the rate matrix $\hat{\boldsymbol{\Gamma}}(\theta)$ in Eq. (52) is determined by ten participating transition rates (four rates from each junction, and two relaxation rates). The resulting eigenvalues of $|g(\theta,\tau)\rangle$ are the solutions of a quartic equation, which is in general very laborious to present analytically.

For symmetric junctions ($R = 1$) with no plasmon relaxation, however, the rate matrix is simplified to

$$\hat{\Gamma}(\theta) = \begin{bmatrix} \gamma_{00} + \gamma_{10} & 0 & -\gamma_{00} z^2 & -\gamma_{01} z^2 \\ 0 & \gamma_{01} + \gamma_{11} & -\gamma_{10} z^2 & -\gamma_{11} z^2 \\ -\gamma_{00} & -\gamma_{01} & \gamma_{00} + \gamma_{10} & 0 \\ -\gamma_{10} & -\gamma_{11} & 0 & \gamma_{01} + \gamma_{11} \end{bmatrix} \tag{66}$$

with the matrix elements $\gamma_{ij} \equiv \Gamma_L(1, i \leftarrow 0, j) = \Gamma_R(0, i \leftarrow 1, j)$. The steady-state probability is then given by

$$|P_4^{(s)}(\infty)\rangle = |g(z, \tau = 0)\rangle = \frac{1}{2(\gamma_{01} + \gamma_{10})} \begin{bmatrix} \gamma_{01} \\ \gamma_{10} \\ \gamma_{01} \\ \gamma_{10} \end{bmatrix}. \tag{67}$$

Solving Eq. (54) with this probability and the rate matrix (66) is laborious but straightforward and one finds

$$G(z, \tau) = e^{-(\gamma_{00} + \gamma_{10} + \gamma_{01} + \gamma_{11})\tau/2} \times \left[\left\{ G_I(z, \tau) \frac{(1+z)^2}{8z} \right\} + \{z \to -z\} \right], \tag{68}$$

with

$$G_I(z, \tau) = \left\{ e^{(\gamma_{00} z + \gamma_{11} z + f_4(z))\tau/2} \left(1 + \frac{A(z)}{f_4(z)} \right) \times \left(1 - \frac{A(z) - f_4(z)}{2(\gamma_{01} + \gamma_{10}) z} \right) \right\} + \{f_4(z) \to -f_4(z)\}, \tag{69}$$

where $A(z)$ and $f_4(z)$ are given by

$$A(z) = \gamma_{00} + \gamma_{10} - \gamma_{01} - \gamma_{11} - (\gamma_{00} - \gamma_{11} - 2\gamma_{01}) z,$$
$$f_4(z) = \sqrt{(\gamma_{00} - \gamma_{11})^2 - 4\gamma_{10}\gamma_{01}} \sqrt{(z-a)^2 + b^2} \tag{70}$$

with dimensionless parameters a, b given by

$$a = \frac{(\gamma_{00} - \gamma_{11})(\gamma_{00} + \gamma_{10} - \gamma_{01} - \gamma_{11})}{(\gamma_{00} - \gamma_{11})^2 - 4\gamma_{10}\gamma_{01}},$$
$$b = \frac{\sqrt{4\gamma_{10}\gamma_{01}}(\gamma_{00} + \gamma_{10} - \gamma_{01} - \gamma_{11})}{(\gamma_{00} - \gamma_{11})^2 - 4\gamma_{10}\gamma_{01}}.$$

Integral of $G_I(z, \tau)$ along the contour $|z| = 1$ contains two branch points at $z_c = a \pm ib$, however, the integral along the branch cuts cancel out due to the symmetry under $[f_4(z) \to -f_4(z)]$. Therefore, the contribution from the branch cuts due to $G_I(z, \tau)$ and $G_I(-z, \tau)$ is zero to the probability $P_4^{(s)}(M, \tau)$, and it is given by the residues only at $z = 0$, i.e., by Eq. (58). The explicit expression of $P_4^{(s)}(M, \tau)$ is cumbersome.

The probability distribution $P_2(M, \tau)$ for the two-state process deviates from Eq. (63) as a function of the asymmetry parameter R and reaches Poissonian in the case of strongly asymmetric junctions. In a similar manner, $P_4^{(s)}(M, \tau)$ deviates from $P_2^{(s)}(M, \tau)$ as a function of ratio of the transition rates γ_{ij}.

6.3. Numerical results

It is worth mentioning that for strongly asymmetric junctions $P(M, \tau)$ is Poissonian in the very low bias regime ($eV < 2\varepsilon_p$), as seen from Eq. (65). It exhibits a crossover at $eV = 2\varepsilon_p$: $P(M, \tau)$ deviates from Poisson distribution for $2\varepsilon_p < eV < 2E_C$ while it is Poissonian for $eV < 2\varepsilon_p$ (at $T = 0$), as shown by the shot noise calculation.

Voltage dependence

The analytic results presented above are useful in interpreting the numerical results in Fig. 9, where probability $P(M, \tau)$ for symmetric junctions ($R = 1$) and $R = 100$, in the case of LL parameter $g = 0.5$ with no plasmon relaxation ($\gamma_p = 0$), is shown as a function of eV and M, that is the number of transported electrons to the right lead during τ such that during this time $\langle M \rangle = I_c \tau = 10$ electrons have passed to the right lead at $eV = 2E_C$.

The peak position of the distribution of $P(M, \tau)$ is roughly linearly proportional to the average particle flow $\langle M \rangle$, and the width is proportional to the shot noise but in a nonlinear manner. In a rough estimate, therefore, the ratio of the peak width to the peak position is proportional to the Fano factor. Two features are shown in the Fig. 9. First, the average particle flow (the peak position) runs with different slope when the bias voltage crosses new energy levels, i.e., at $eV = 2\varepsilon_p$ and $eV = 2E_C$, that is consistent with the $I - V$ study (compare Fig. 9,*b* with Fig. 3). Notice $E_C = \varepsilon_p / g = 2\varepsilon_p$ for $g = 0.5$. Second, the width of the distribution increases with increasing voltage, with different characteristics categorized by $eV = 2\varepsilon_p$ and $eV = 2E_C$. Especially in the bias regime $eV > 2E_C$ in which several charge states participate to the charge transport, for the highly asymmetric case, the peak runs very fast while its width does not show noticeable increase. It causes the dramatic peak structure in the Fano factor around $eV = 2E_C$ as discussed in Sec. 5.

The deviation of the distribution of probability $P(M, \tau)$ due to the nonequilibrium plasmons from its low voltage (equilibrium) counterpart is shown in the insets. Notice in the low-bias regime $eV < 2\varepsilon_p$, it follows Eq. (63) for the symmetric case (Fig. 9,*a*, inset I), and the Poissonian distribution (65) for the highly

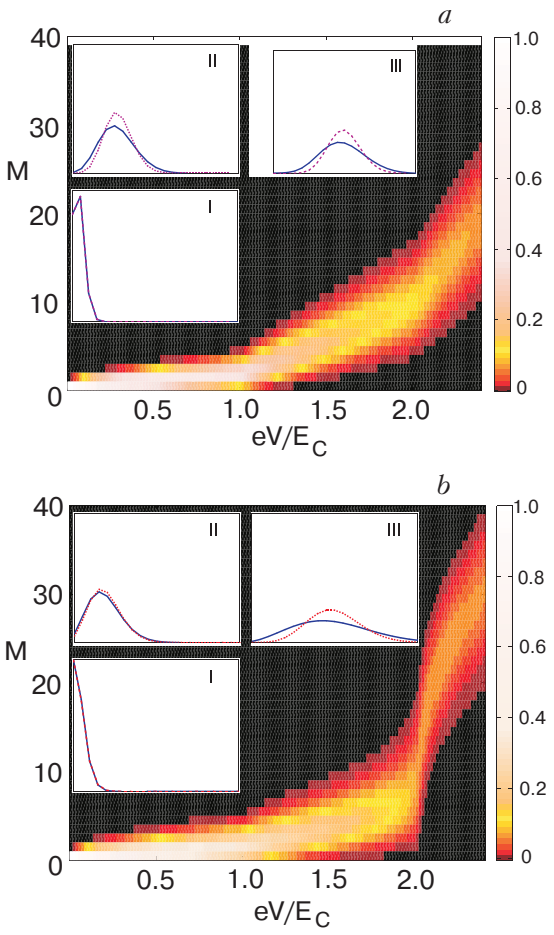

Fig. 9. Probability $P(M,\tau)$ with no plasmon relaxation ($\gamma_p = 0$) during the time ($\tau = 10/I_c$, where I_c is the particle current at $eV = 2E_C$ with no plasmon relaxation ($\gamma_p = 0$): for symmetric junctions ($R = 1$) (*a*) and for a highly asymmetric junctions ($R = 100$) (*b*). Here $g = 0.5$, $N_G = 1/2$, and $T = 0$. Inset shows cross-sectional image of $P(M,\tau)$ (blue solid line) as a function of M and the reference distribution function (*a*) Eq. (63) (magenta dashed line) and (*b*) the Poisson distribution Eq. (65) (red dashed), at $eV = 0.5E_C$ (I), $eV = 1.5E_C$ (II), and $eV = 2E_C$ (III).

asymmetric case (Fig. 9,*b*, inset I). The deviation is already noticeable at $eV = 3\varepsilon_p = 1.5E_C$ for $R = 1$ (inset II in Fig. 9,*a*), while it deviates strongly around $eV = 2E_C$ for $R = 100$ (inset III in Fig. 9,*a*).

Interaction strength dependence

We have concluded in Sec. 5 that shot noise shows most dramatic behavior around $eV = 2E_C$ due to interplay between the nonequilibrium plasmons and the charge excitations. To see its consequence in FCS, we plot in Fig. 10 the probability $P(M,\tau)$ as a function of the particle number M and the interaction parameter g for $\tau = 10e/I(eV = 2E_C, \gamma_p = 0)$ with no plasmon relaxation and with fast plasmon relaxation.

The main message of Fig. 10,*a* is that the shot noise enhancement, i.e., the broadening of the distribution

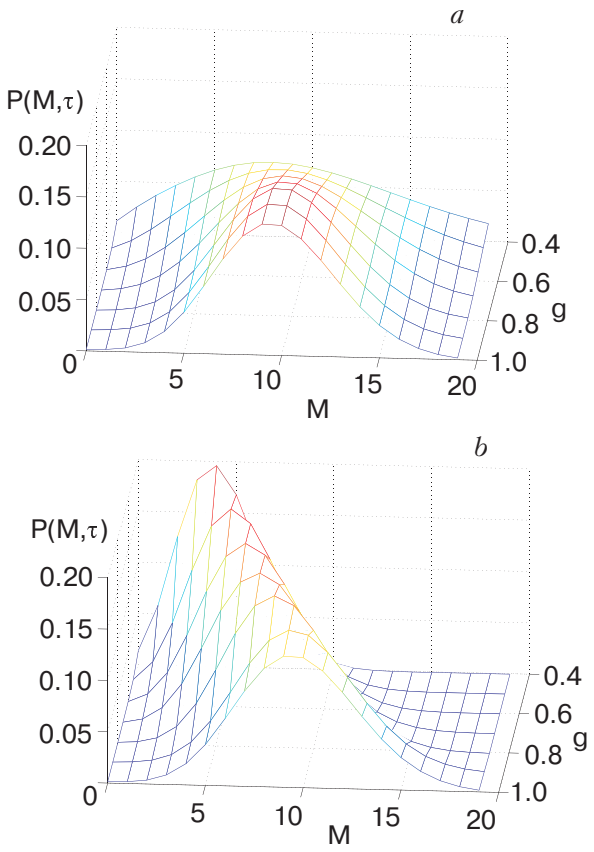

Fig. 10. The probability $P(M,\tau)$ that M electrons have passed through the right junction during the time $\tau = 10/I_0$, where I_0 is the particle current with no plasmon relaxation ($\gamma_p = 0$); with no plasmon relaxation ($\gamma_p = 0$) (*a*) and with fast plasmon relaxation ($\gamma_p = 10^4$) (*b*). Here $eV = 2E_C$, $R = 100$, $N_G = 1/2$ and $T = 0$.

curve, is significant in the strong interaction regime with gradual increase with decreasing g. Fast plasmon relaxation consequently suppresses the average current and the shot noise dramatically as shown in Fig. 10,*b* implying the Fano factor enhancement is lost. Effectively, the probability distribution of $P(M,\tau)$ for different interaction parameters maps on each other almost identically if the time duration is chosen such that $\langle M \rangle$ equals for all g.

7. Conclusions

We have studied different transport properties of a Luttinger-liquid single-electron transistor including average current, shot noise, and full counting statistics, within the conventional sequential tunneling approach.

At finite bias voltages, the occupation probabilities of the many-body states on the central segment is found to follow a highly nonequilibrium distribution. The energy is transferred between the leads and the quantum dot by the tunneling electrons, and the electronic energy is dispersed into the plasmonic collective

excitations after the tunneling event. In the case of nearly symmetric barriers, the distribution of the occupation probabilities of the nonequilibrium plasmons shows impressive contrast depending on the interaction strength: In the weakly interacting regime, it is a complicated function of the many-body occupation configuration, while in the strongly interacting regime, the occupation probabilities are determined almost entirely by the state energies and the bias voltage, and follow a universal distribution resembling Gibbs (equilibrium) distribution. This feature in the strong interaction regime fades out with the increasing asymmetry of the tunnel-barriers.

We have studied the consequences of these nonequilibrium plasmons on the average current, shot noise, and counting statistics. Most importantly, we find that the average current is increased, shot noise is enhanced beyond the Poisson limit, and full counting statistics deviates strongly from the Poisson distribution. These nonequilibrium effects are pronounced especially in the strong interaction regime, i.e. $g \lesssim 0.5$. The overall transport properties are determined by a balance between phenomena associated with nonequilibrium plasmon distribution that tend to increase noise, and involvement of several charge states and the ensuing correlations that tend to decrease noise. The result of this competition is, for instance, a nonmonotonic voltage dependence of the Fano factor.

At the lowest voltages when charge can be transported through the system, the plasmon excitations are suppressed, and the Fano factor is determined by charge oscillations between the two lowest zero-modes. Charge correlations are maximized when the tunneling-in and tunneling-out rates are equal, which for symmetric junctions occurs at gate charge $N_G = 1/2$. At these gate charges the Fano factor acquires its lowest value which at low voltages is given by a half of the Poisson value, known as $1/2$ suppression, as only two states are involved in the transport, at somewhat larger voltages increases beyond the Poisson limit as plasmon excitations are allowed, and at even higher voltages exhibits a local minimum when additional charge states are important. If the nonequilibrium plasmon effects are suppressed, e.g., by fast plasmon relaxation, only the charge excitations and the ensuing correlation effects survive, and the Fano factor is reduced below its low-voltage value. The nonequilibrium plasmon effects are also suppressed in the noninteracting limit.

Acknowledgments

This work has been supported by the Swedish Foundation for Strategic Research through the CARAMEL consortium, STINT, the SKORE-A program, the eSSC at Postech, and the SK-Fund. J.U. Kim acknowledges partial financial support from Stiftelsen Fru Mary von Sydows, född Wijk, donationsfond. I.V. Krive gratefully acknowledges the hospitality of the Department of Applied Physies at Chalmers University of Technology.

Appendix A: The transition amplitudes in the quantum dot

In this appendix, we derive the transition amplitudes, Eqs. (15) and (16). As shown in Eq. (14), the zero-mode overlap of the QD transition amplitude is either unity or zero. Therefore, we focus on the overlap of the plasmon states. It is enough to consider

$$|\langle\{n'\}|\Psi_D^\dagger(X_\ell)|\{n\}\rangle|^2, \quad X_\ell = X_L, X_R$$

due to the symmetry between matrix elements of tunneling-in and tunneling-out transitions, as in Eq. (15),

$$|\langle\{n'\}|\Psi^\dagger(X_\ell)|\{n\}\rangle|^2 = \sum_{r=\pm}[|\langle\{n'\}|\psi_r^\dagger(X_\ell)|\{n\}\rangle|^2 +$$
$$+ \langle\{n'\}|\psi_r^\dagger(X_\ell)|\{n\}\rangle\langle\{n\}|\psi_{-r}(X_\ell)|\{n'\}\rangle] =$$
$$= 2|\langle\{n'\}|\psi_r^\dagger(X_\ell)|\{n\}\rangle|^2, \qquad (A.1)$$

where $r = +(-)$ denotes the right (left)-moving component, and the cross terms of oppositely moving components cancel out due to fermionic anti-commutation relations.

The transition amplitudes at X_L is identical to that at X_R. For simplicity, we consider the case at $X_L = 0$ only. The overlap elements of the many-body occupations $\langle\{n\}| = \langle n_1, n_2, \ldots, n_m, \ldots|$ and $|\{n'\}\rangle = |n'_1, n'_2, \ldots, n'_m, \ldots\rangle$ are

$$|\langle\{n\}|\psi_r^\dagger(x=0)|\{n'\}\rangle|^2 = \frac{1}{2\pi\Lambda}\prod_{m=1}^{\infty}|\langle n_m|\varphi_m|n'_m\rangle|^2, \qquad (A.2)$$

where $\varphi_m = \exp[\lambda_m(b_m + b_m^\dagger)]$ with $\lambda_m = -i/\sqrt{gmM}$ is the bosonized field operator at an edge of the wire with open boundary conditions (see for instance Ref. 44). Here g is the interaction parameter, m is the mode index (and the integer momentum of it), and M is the number of transport sectors; if $M > 1$, the contributions of the different sectors must be multiplied. The operators b_m and $b_m^\dagger$ denote plasmon annihilation and creation and Λ is a high energy cut-off.

Using the Baker–Haussdorf formula

$$\varphi_m = \exp[\lambda_m(a_m + a_m^\dagger)] = e^{-\frac{\lambda_m^2}{2}} e^{\lambda_m a_m} e^{\lambda_m a_m^\dagger}, \qquad (A.3)$$

and the harmonic oscillator states

$$|n\rangle = \frac{(a^\dagger)^n}{\sqrt{n!}}|0\rangle, \quad \langle n| = \langle 0|\frac{a^n}{\sqrt{n!}}, \qquad (A.4)$$

one can show that, if $n \le n'$,

$$|\langle n|\varphi|n'\rangle|^2 = e^{|\lambda|^2}\,\frac{|\lambda|^{2(n-n')}}{n!\,n'!}\left(\frac{n!}{(n-n')!}\right)^2 \times$$

$$\times\,\Phi(n+1,\,n-n'+1;\,-|\lambda|^2)^2, \qquad \text{(A.5)}$$

where $\Phi(x,x';z)$ is a degenerate hypergeometric function defined by [77]

$$\Phi(x,x';z) = \left[\sum_{\ell=0}^{\infty}\frac{z^\ell}{\ell!}\,\frac{(x-1+\ell)!}{(x-1)!}\,\frac{(x'-1)!}{(x'-1+\ell)!}\right]. \qquad \text{(A.6)}$$

If $n' \le n$, the indices n and n' are exchanged in Eq. (A.5). The function $\Phi(x,x';z)$ is a solution of the equation

$$z\partial_z^2\Phi + (x'-z)\partial_z\Phi - x\Phi = 0.$$

By solving this differential equation with the proper normalization constant, one obtains

$$\Phi(n+1,n-n'+1;\,-|\lambda|^2) = \frac{n'!(n-n')!}{n!}\,e^{-|\lambda|^2}\,L_{n'}^{n-n'}(|\lambda|^2),$$

where $L_a^b(y)$ is the Laguerre polynomials [77]. In terms of the Laguerre polynomials, therefore, the transition amplitude (A.5) is written by

$$|\langle n_m|\varphi_m|n'_m\rangle|^2 = \frac{e^{-1/gmM}}{(gmM)^{|n'_m-n_m|}}\,\frac{n_m^{(<)}!}{n_m^{(>)}!}\times$$

$$\times\left[L_{n_m^{(<)}}^{|n'_m-n_m|}\left(\frac{1}{gmM}\right)\right]^2, \qquad \text{(A.7)}$$

where $n^{(<)} = \min(n',n)$ and $n^{(>)} = \max(n',n)$.

We introduce a high frequency cut-off $m_c \sim k_F L_D/\pi$ to cure the vanishing contribution due to $e^{-1/gmM}$,

$$\frac{1}{2\pi\Lambda}\prod_{m=1}^{m_c} e^{-1/4mg} \to \frac{1}{2L_D}\left(\frac{\pi\Lambda_c}{L_D}\right)^\alpha, \qquad \text{(A.8)}$$

where the exponent is $\alpha = (g^{-1}-1)/M$. We arrive at the desired form of the on-dot transition matrix elements,

$$|\{n'\}|\Psi_a^\dagger(X_\ell)|\{n\}\rangle|^2 = \frac{1}{L_D}\left(\frac{\pi\Lambda}{L_D}\right)^\alpha \times$$

$$\times\prod_\nu\prod_{m=1}^{\infty}\left(\frac{1}{g_\nu mM}\right)^{|n'_m-n_m|}\frac{n_m^{(<)}!}{n_m^{(>)}!}\left[L_{n_m^{(<)}}^{|n'_m-n_m|}\left(\frac{1}{g_\nu mM}\right)\right]^2, \qquad \text{(A.9)}$$

Appendix B: Universal occupation probability

In this appendix, we derive the universal distribution of the occupation probability, which becomes Eq. (26) in the leading order approximation.

Since the occupation probability of the plasmon many-body states is a function of the state energy in the strong interaction regime, we introduce the dimensionless energy $n = \sum_m mn_m$ of the state with $\{n\} = (n_1,n_2,\ldots,n_m,\ldots)$ plasmon occupations. Excluding the zero mode energy, therefore, the energy of the state $\{n\}$ is given by $E_D(\{n\}) = E_D(n) = n\varepsilon_p$ with the state degeneracy $D(n)$, i.e., the number of many-body states n satisfying $n = \sum_m mn_m$, asymptotically following the Hardy–Ramanujan formula [78]

$$D(n) \simeq e^{\pi\sqrt{2n/3}}/(4\sqrt{3}n). \qquad \text{(B.1)}$$

We denote n_{sd} by the corresponding dimensionless bias voltage $eV = n_{sd}\varepsilon_p$.

We obtain an analytic approximation to the occupation probability $P(n)$ at zero temperature by setting the on-dot transition elements in (15) to unity and considering the scattering-in and scattering-out processes for a particular many-body state $\{n\}$.

The total scattering rates at zero temperature are given by a simple power-law Eq. (13),

$$\Gamma(n \leftarrow m) = \Theta(-n+m-n_{sd}/2)(-n+m-n_{sd}/2)^\alpha +$$

$$+\,\Theta(-n+m+n_{sd}/2)(-n+m+n_{sd}/2)^\alpha \approx$$

$$\approx \Theta(-n+m-n_{sd}/2)(-n+m-n_{sd}/2)^\alpha, \qquad \text{(B.2)}$$

where the constant factor in Eq. (13) is set to unity.

The master equation now reads

$$\frac{\partial}{\partial t}P(n) = \sum_m [P(m)D(m)\Gamma(m \to n) - P(n)D(m)\Gamma(n \to m)]. \qquad \text{(B.3)}$$

To solve this master equation, we assume an ansatz of a power-law

$$P(m) = P(n)q_n^{m-n}. \qquad \text{(B.4)}$$

In the steady-state, master equation (B.3) in terms of this ansatz becomes

$$\sum_{m=m_i}^{\infty}(m-n+n_{sd}/2)^\alpha D(m)q_n^{m-n} \approx$$

$$\approx \sum_{m'=0}^{n+n_{sd}/2}(n-m'+n_{sd}/2)^\alpha D(m'), \qquad \text{(B.5)}$$

in which the sum in the LHS runs from $m_i = \max(0, n - n_{sd}/2)$, where $\max(x,x')$ gives larger of x and x'.

Using a saddle point integral approximation

$$\int e^{f(x)}dx \approx e^{f(x_0)}\int e^{\frac{1}{2}f''(x_0)(x-x_0)^2}dx, \quad \text{(B.6)}$$

$$\text{if } f'(x_0)=0, \quad f''(x_0)<0\ ,$$

we solve Eq. (B.5) to obtain an equation for $\ln q_n$ and find that for a large n,

$$\exp(z)/z \approx \sqrt{n}\exp(F(n)), \quad \text{(B.7)}$$

where

$$z=\frac{|\ln q|}{C_\alpha}, \quad C_\alpha=\frac{\alpha+1}{n_{sd}/2},$$

and $F(n)$ is a slowly varying function of n for $n >> 1$,

$$F(n)=\sqrt{\frac{2}{3}}\frac{\pi}{C_\alpha\sqrt{n}}+\ln\left[\frac{\sqrt{6}}{\pi}C_\alpha\right]+\frac{n_{sd}}{n}\left(\frac{1}{4}-\frac{1}{\alpha+1}\right). \quad \text{(B.8)}$$

We assume an ansatz for the solution of z in Eq. (B.7),

$$z=(\ln n)/2+F(n)+\sqrt{(\ln n)/2+F(n)-K}+\eta \quad \text{(B.9)}$$

and find a constant K which minimizes the correction term η. Putting this ansatz into Eq. (B.7) and solving the equation for η, we find at $K \approx 0.8$, that the correction term η is negligibly small ($\eta \approx 0.01$).

Noting $f(n)=\sqrt{(\ln n)/2+F(n)-K}$ is almost linear function in the regime of our interest ($3 \lesssim n \lesssim 15$), we linearize it around a value $n=n_0$ (for instance, $n_0=9$), $f(n) \approx f'(n_0)(n-n_0)+f(n_0)$, and solve Eq. (B.7) by ansatz (B.9) with above linearized form;

$$-\frac{\ln q_n}{C_\alpha} \approx \frac{1}{2}\ln n + F(n) + f'(n_0)n + f(n_0) - f'(n_0)n_0. \quad \text{(B.10)}$$

Apply $\partial_m \ln[P(m)] \approx \ln[q_n]$ to Eq. (B.10), and solve the integral equation for $\ln[P(n)]$,

$$\ln[P(n)] \approx -C_\alpha\int^n dn\,[(\ln n)/2+F(n)+ + f'(n_0)n+f(n_0)-f'(n_0)n_0]\ . \quad \text{(B.11)}$$

The leading order approximation $P^{(0)}(n)$ to the probability $P(n)$ of the average occupation from this integral results in Eq. (26)

$$P^{(0)}(n)=Z^{-1}\,n^{-\frac{3}{2}\frac{\alpha+1}{n_{sd}}n}=Z^{-1}e^{-\frac{3}{2}\frac{\alpha+1}{n_{sd}}n\log n}, \quad \text{(B.12)}$$

where Z is the partition function.

A more accurate approximation $P^{(1)}(n)$ can be derived by solving the integral Eq. (B.11) to a higher degree of precision, which yields

$$P^{(1)}=Z^{-1}\left(\sqrt{n}\left(n+\frac{n_{sd}}{2}\right)\right)^{-C_\alpha n/2}\left(\frac{\sqrt{6}}{\pi}C_\alpha\right)^{-C_\alpha n}\exp\left(-C_\alpha n\left[F(n_0)-K+\frac{\ln 3}{2}-\frac{3}{4}\right]\right)\times$$
$$\times\exp\left(-\frac{4\pi}{\sqrt{6}}\sqrt{n}\right)\left(\frac{n-n_{sd}/2}{n+n_{sd}/2}\right)^{-2n/n_{sd}}\left(n+\frac{n_{sd}}{2}\right)^{-(\alpha+1)/2}\left(n^2-\left(\frac{n_{sd}}{2}\right)^2\right), \quad \text{(B.13)}$$

where $n_0=9$ is used and $f(n_0) \approx f^2(n_0)$ with minor correction is utilized for formal simplicity. Note the first term with normalization constant Z approaches $P^{(0)}(n)$ in Eq. (B.12) as $n/n_{sd} \to 0$, noticing $C_\alpha=2(\alpha+1)/n_{sd}$. The integral equation (B.11) can be solved even without approximating on $f(n)$, with the expense of more cumbersome appearance of $P(n)$.

1. S. Tomonaga, *Prog. Theor. Phys.* **5**, 544 (1950).
2. J.M. Luttinger, *J. Math. Phys.* **4**, 1154 (1963).
3. F.D.M. Haldane, *J. Phys.* **C14**, 2585 (1981).
4. A.O. Gogolin, A.A. Nersesyan, and A.M. Tsvelik, *Bosonization and Strongly Correlated Systems*, Cambridge University Press, Cambridge (1998).
5. A.M. Chang, L.N. Pfeiffer, and K.W. West, *Phys. Rev. Lett.* **77**, 2538 (1996).
6. S.J. Tans, M.H. Devoret, H. Dai, A. Thess, R.E. Smalley, L.J. Geerligs, and C. Dekker, *Nature (London)* **386**, 474 (1997).
7. M. Bockrath, D.H. Cobden, J. Lu, A.G. Rinzler, R.E. Smalley, L. Balents, and P.L. McEuen, *Nature (London)* **397**, 598 (1999).
8. Z. Yao, H.W.C. Postma, L. Balents, and C. Dekker, *Nature (London)* **402**, 273 (1999).
9. T. Lorenz, M. Hofmann, M. Grüninger, A. Freimuth, G.S. Uhrig, M. Dumm, and M. Dressel, *Nature (London)* **418**, 614 (2002).
10. G.L. Ingold and Y.V. Nazarov, in *Single Charge Tunneling, Coulomb Blockade Phenomena in Nanostructures*, H. Grabert and M.H. Devoret (eds.), Plenum Press, New York (1992), chap. 2.
11. O.M. Auslaender, A. Yacoby, R. De Picciotto, K.W. Baldwin, L.N. Pfeiffer, and K.W. West, *Phys. Rev. Lett.* **84**, 1764 (2000).

12. H.W.C. Postma, T. Teepen, Z. Yao, M. Grifoni, and C. Dekker, *Science* **293**, 76 (2001).
13. C.L. Kane and M.P.A. Fisher, *Phys. Rev.* **B46**, 7268 (1992).
14. A. Furusaki, *Phys. Rev.* **B57**, 7141 (1998).
15. M. Thorwart, M. Grifoni, G. Cuniberti, H.W.C. Postma, and C. Dekker, *Phys. Rev. Lett.* **89**, 196402 (2002).
16. S. Hügle and R. Egger, *Europhys. Lett.* **66**, 565 (2004).
17. Y.V. Nazarov and L.I. Glazman, *Phys. Rev. Lett.* **91**, 126804 (2003).
18. D.G. Polyakov and I.V. Gornyi, *Phys. Rev.* **B68**, 035421 (2003).
19. V. Meden, T. Enss, S. Andergassen, W. Metzner, and K. Schoenhammer, *cond-mat/0403655* (2004).
20. T. Enss, V. Meden, S. Andergassen, X. Barnabe-Theriault, W. Metzner, and K. Schönhammer, *cond-mat/0411310* (2004).
21. A. Braggio, M. Grifoni, M. Sassetti, and F. Napoli, *Europhys. Lett.* **50**, 236 (2000).
22. A. Braggio, R. Fazio, and M. Sassetti, *Phys. Rev.* **B67**, 233308 (2003).
23. J.U. Kim, I.V. Krive, and J.M. Kinaret, *Phys. Rev. Lett.* **90**, 176401 (2003).
24. J.U. Kim, J.M. Kinaret, and M.S. Choi, *J. Phys.: Condens. Matter* **17**, 3815 (2005).
25. J.W. Wilkins, S. Hershfield, J.H. Davies, P. Hyldgaard, and C.J. Stanton, *Phys. Scripta* **T42**, 115 (1992).
26. J.H. Davies, P. Hyldgaard, S. Hershfield, and J.W. Wilkins, *Phys. Rev.* **B46**, 9620 (1992).
27. S. Hershfield, J.H. Davies, P. Hyldgaard, C.J. Stanton, and J.W. Wilkins, *Phys. Rev.* **B47**, 1967 (1993).
28. A.N. Korotkov, *Phys. Rev.* **B49**, 10381 (1994).
29. E.V. Sukhorukov, G. Burkard, and D. Loss, *Phys. Rev.* **B63**, 125315 (2001).
30. M.J.M. De Jong and C.W.J. Beenakker, in *NATO ASI Series* Vol. 345, L. Sohn, L. Kouwenhoven, and G. Schön (eds.), Kluwer Academic Publishers, Dordrecht (1997), p. 225.
31. Y.M. Blanter and M. Büttiker, *Phys. Rep.* **336**, 1 (2000).
32. D. Tománek, private communication (2004).
33. I.O. Kulik and R.I. Shekhter, *Sov. Phys. JETP* **41**, 308 (1975).
34. L.I. Glazman and R.I. Shekhter, *J. Phys.: Condens. Matter* **1**, 5811 (1989).
35. R. Egger and H. Grabert, *Phys. Rev. Lett.* **77**, 538 (1996); *ibid.* **80**, 2255(E) (1998).
36. R. Egger and H. Grabert, *Phys. Rev.* **B58**, 10761 (1998).
37. J. Voit, *Rep. Prog. Phys.* **58**, 1116 (1995).
38. C. Kane, L. Balents, and M.P.A. Fisher, *Phys. Rev. Lett.* **79**, 5086 (1997).
39. R. Egger and A.O. Gogolin, *Phys. Rev. Lett.* **79**, 5082 (1997).
40. M. Sassetti, G. Cuniberti, and B. Kramer, *Solid State Commun.* **101**, 915 (1997).
41. M. Sassetti and B. Kramer, *Phys. Rev.* **B55**, 9306 (1997).
42. M. Fabrizio and A.O. Gogolin, *Phys. Rev.* **B51**, 17827 (1995).
43. S. Eggert, H. Johannesson, and A.E. Mattsson, *Phys. Rev. Lett.* **76**, 1505 (1996).
44. A.E. Mattsson, S. Eggert, and H. Johannesson, *Phys. Rev.* **B56**, 15615 (1997).
45. K.A. Matveev and L.I. Glazman, *Phys. Rev. Lett.* **70**, 990 (1993).
46. K.A. Matveev and L.I. Glazman, *Physica* **B189**, 266 (1993).
47. A. Braggio, M. Sassetti, and B. Kramer, *Phys. Rev. Lett.* **87**, 146820 (2001).
48. F. Cavaliere, A. Braggio, J.T. Stockburger, M. Sassetti, and B. Kramer, *Phys. Rev. Lett.* **93**, 036803 (2004).
49. S. Kogan, *Electronic Noise and Fluctuations in Solids*, Cambridge University Press, Cambridge (1996).
50. C. Beenakker and C. Schönenberger, *Phys. Today* **56**, 37 (2003).
51. R. Deblock, E. Onac, L. Gurevich, and L.P. Kouwenhoven, *Science* **301**, 203 (2003).
52. M.S. Choi, F. Plastina, and R. Fazio, *Phys. Rev. Lett.* **87**, 116601 (2001).
53. M.S. Choi, F. Plastina, and R. Fazio, *Phys. Rev.* **B67**, 045105 (2003).
54. C.L. Kane and M.P.A. Fisher, *Phys. Rev. Lett.* **72**, 724 (1994).
55. L. Saminadayar, D.C. Glattli, Y. Jin, and B. Etienne, *Phys. Rev. Lett.* **79**, 2526 (1997).
56. R. De Picciotto, M. Reznikov, M. Heiblum, V. Umansky, G. Bunin, and D. Mahalu, *Nature (London)* **389**, 162 (1997).
57. E. Comforti, Y.C. Chung, M. Heiblum, V. Umansky, and D. Mahalu, *Nature (London)* **416**, 515 (2002).
58. L.Y. Chen and C.S. Ting, *Phys. Rev.* **B43**, 4534 (1991).
59. O.L. Bo and Y. Galperin, *J. Phys.: Condens. Matter* **8**, 3033 (1996).
60. L.Y. Chen and C.S. Ting, *Phys. Rev.* **B46**, 4714 (1992).
61. L.Y. Chen, *Phys. Rev.* **B48**, 4914 (1993).
62. A.N. Korotkov, D.V. Averin, K.K. Likharev, and S.A. Vasenko, in *Single Electron Tunneling and Mesoscopic Devices*, H. Koch and H. Lübbrig (eds.), Springer, Berlin (1992), p. 45.
63. U. Hanke, Y.M. Galperin, and K.A. Chao, *Phys. Rev.* **B50**, 1595 (1994).
64. H. Birk, M.J.M. de Jong, and C. Schönenberger, *Phys. Rev. Lett.* **75**, 1610 (1995).
65. A. Isacsson and T. Nord, *Europhys. Lett.* **66**, 708 (2004).
66. A. Thielmann, M.H. Hettler, J. König, and G. Schön, *cond-mat/0501534* (2005).
67. H.A. Engel and D. Loss, *Phys. Rev. Lett.* **93**, 136602 (2004).

68. S.S. Safonov, A.K. Savchenko, D.A. Bagrets, O.N. Jouravlev, Y.V. Nazarov, E.H. Linfield, and D.A. Ritchie, *Phys. Rev. Lett*. **91**, 136801 (2003).
69. T. Novotny, A. Donarini, C. Flindt, and A.P. Jauho, *Phys. Rev. Lett*. **92**, 248302 (2004).
70. L.S. Levitov and G.B. Lesovik, *JETP Lett*. **58**, 233 (1993).
71. B.A. Muzykantskii and D.E. Khmelnitskii, *Phys. Rev*. **B50**, 3982 (1994).
72. H. Lee, L.S. Levitov, and A.Y. Yakovets, *Phys. Rev*. **B51**, 4079 (1995).
73. B. Reulet, J. Senzier, and D.E. Prober, *Phys. Rev. Lett*. **91**, 196601 (2003).
74. L.S. Levitov and G.B. Lesovik, *Phys. Rev*. **B70**, 115305 (2004), also at *cond-mat/0111057*.
75. C.W.J. Beenakker, M. Kindermann, and Y.V. Nazarov, *Phys. Rev. Lett*. **90**, 176802 (2003).
76. M.J.M. de Jong, *Phys. Rev*. **B54**, 8144 (1996).
77. I.S. Gradshteyn and I.M. Ryzhik, *Table of Integrals, Series, and Products*, Academic Press, London (1980).
78. G.H. Hardy and S. Ramanujan, *Proc. London Math. Soc*. **17**, 75 (1918).